



# 1 **Is the Atlantic Ocean driving the recent variability in South** 2 **Asian dust?**

3 Priyanka Banerjee<sup>1</sup>, Sreedharan Krishnakumari Satheesh<sup>1,2</sup>, Krishnaswamy Krishna Moorthy<sup>2</sup>

4 <sup>1</sup>Divecha Centre for Climate Change, Indian Institute of Science, Bangalore, India

5 <sup>2</sup>Centre for Atmospheric and Oceanic Sciences, Indian Institute of Science, Bangalore, India

6 *Correspondence to:* Priyanka Banerjee ([pbanerjee.ocean@gmail.com](mailto:pbanerjee.ocean@gmail.com))

7

## 8 **Abstract**

9 This study investigates the large-scale factors controlling interannual variability of dust aerosols over South  
10 Asia during 2001-2018. We use a parameter  $DA_{\%}$ , which refers to the frequency of days in a year when high  
11 dust activity is experienced over a region, as determined by combination of satellite aerosol optical depth and  
12 Angstrom exponent. While positive sea surface temperature (SST) anomaly in the central Pacific Ocean has  
13 been important in controlling  $DA_{\%}$  over South Asia during 2001-2010; in recent years the North Atlantic Ocean  
14 has assumed a dominant role. Specifically, high  $DA_{\%}$  is associated with warming in the mid-latitude and cooling  
15 in the sub-tropical North Atlantic SSTs: the two southern arms of the North Atlantic SST tripole pattern. This  
16 shift towards a dominant role of the North Atlantic SST in controlling  $DA_{\%}$  over South Asia is associated with a  
17 recent shift towards persistently positive phase of the North Atlantic Oscillation (NAO) and a resultant positive  
18 phase of the spring-time SST tripole pattern. Interestingly, there has also been a shift in the relation between the  
19 two southern arms of the SST tripole and NAO, which has resulted in weakening of the southwest monsoon  
20 circulation over the northern Indian Ocean and strengthening of the dust-carrying westerlies and northerlies in  
21 the lower and mid-troposphere. Simulations with an earth system model show that anomalous transport due to  
22 the North Atlantic SST tripole pattern can result in 10% (20%) increase in dust optical depth (concentration at  
23 800 hPa) over South Asia during May-September; with increases as much as 30% (50%) during the month of  
24 June.

25

## 26 **1 Introduction**

27 South Asia is believed to be highly vulnerable to the long-term impacts of climate change (Stocker et al., 2013).  
28 One of the ways in which the impact of climate change is felt in this region is via aerosol feedback on the  
29 regional climate (e.g., Satheesh and Ramanathan, 2000; Ramanathan et al., 2005; Bollasina et al., 2011).  
30 Mineral dust is the most important aerosol component (by mass) present in this region (e.g., Ginoux et al., 2012;  
31 Jin et al., 2018a; Banerjee et al., 2019). Several studies during the last two decades have shown that mineral dust  
32 can influence different aspects of the climate of South Asia with the largest focus given to dust impact on  
33 radiative balance (e.g., Deepshikha et al., 2006; Zhu et al., 2007; Pandithurai et al., 2008) and the southwest  
34 monsoon (SWM) precipitation (Vinoj et al., 2014; Jin et al., 2014; Solmon et al., 2015). However, to better  
35 appreciate dust-climate feedback, it is important to understand what large-scale factors control dust emission



36 and transport in this region and, if there are long-term changes in these controlling factors. At present, there is  
37 very little understanding of these factors, sometimes with lack of consensus among the studies.

38 There are some recent indirect evidences of El Nino/La Nina influencing dust fluxes over South Asia. For  
39 example, Kim et al. (2016) have reported that La Nina conditions are associated with increased absorbing  
40 aerosols over northwest India which, in turn, leads to positive feedback on the SWM precipitation. On the  
41 contrary, Abish and Mohankumar (2013) argued that increased zonal transport and subsidence over India during  
42 El Nino years can lead to enhanced absorbing aerosols like dust over India. A few other studies have shown that  
43 over Southwest Asia, variability of dust aerosols is controlled by climatic factors like El Nino/La Nina at  
44 interannual timescale (Notaro et al., 2015; Yu et al., 2015; Banerjee and Prasanna Kumar, 2016) and by Pacific  
45 Decadal Oscillation (PDO) at interdecadal timescale (Notaro et al., 2015; Yu et al., 2015; Pu and Ginoux, 2016).  
46 Eastward transport of dust from Southwest Asia by the mid-level westerlies are shown to contribute about 50%  
47 to the total dust optical depth over the Indo-Gangetic plain of South Asia (Banerjee et al., 2019) and can  
48 influence its trend over this region. During the beginning of the 21<sup>st</sup> century, a positive trend in SWM  
49 precipitation due to the negative phase of Interdecadal Pacific Oscillation (Huang et al., 2020) has resulted in a  
50 negative trend of dust aerosol over South Asia (Pandey et al., 2017; Jin and Wang, 2018b). Ice core records in  
51 the central Himalayas have shown an inverse relation between the SWM precipitation and dust deposition  
52 (Thompson et al., 2000). During winter season, aerosol optical depth over northern India is shown to be  
53 positively correlated to simultaneous central Pacific Nino index and negatively correlated to Antarctic  
54 Oscillation during the preceding autumn (Gao et al., 2019).

55 The main dust source regions over South Asia are spread across the Thar Desert and the Indo-Gangetic plain in  
56 India and Pakistan; the Makran coast and the Hamun-I-Mashkel in Pakistan; the Margo Desert and the Rigestan  
57 Desert in Afghanistan (Walker et al., 2009; Ginoux et al., 2012). The Margo Desert, the Rigestan Desert and the  
58 Hamun-I-Mashkel receive predominantly winter precipitation from the Mediterranean low-pressure systems  
59 travelling eastwards. Rest of the regions receive summer precipitation from the SWM system, although the total  
60 amount of precipitation received is very low. It has been shown by several studies that one of the major factors  
61 controlling the interannual variability of the SWM rainfall is El Nino/La Nina with developing El Nino  
62 conditions over the Pacific Ocean leading to weakening of the SWM moisture influx (e.g., Sikka, 1980;  
63 Rasmusson and Carpenter, 1983; Ashok et al., 2004). Tropical Pacific Ocean warming (cooling) is also  
64 responsible for wetter (drier) than normal conditions over the winter precipitation region in Southwest Asia  
65 (Barlow et al., 2002; Mariotti, 2002). This implies that the conditions prevailing over the Pacific Ocean has an  
66 important role in controlling the level of dust activity over the northern Indian Ocean (IO) and South Asia either  
67 directly through precipitation impact on dust emission and/or indirectly through dust transport from Southwest  
68 Asia. However, in the backdrop of global warming and the internal variability of the Pacific Ocean at different  
69 timescales (e.g., Kosaka and Xie, 2016; Deser et al., 2017a), the well-known El Nino-monsoon relation has  
70 undergone changes in the recent decades. Since the late 1970s, the relation between El Nino and negative  
71 rainfall anomaly over India has become less significant, possibly, due to the greater rate of warming of the  
72 Eurasian landmass in the recent years compared to the IO or due to the cooling of the Pacific Ocean (Kumar et  
73 al., 1999; Kinter et al., 2002). Simultaneously, the Atlantic Ocean has assumed a stronger role in modulating the  
74 monsoon circulation over the northern IO (Chang et al., 2001; Kucharski et al., 2007; Kucharski et al., 2008).



75 While some studies have shown the importance of the sea surface temperature (SST) along the south equatorial  
76 Atlantic (Kucharski et al., 2007; Kucharski et al., 2008), other studies have shown that positive SST anomalies  
77 over the western North Atlantic centered on 40°N latitude can lead to positive anomalies of monsoon over India  
78 (Srivastava et al., 2002; Rajeevan and Sridhar, 2008). Over the North Atlantic Ocean, the dominant mode of sea  
79 level pressure variability during winter is the North Atlantic Oscillation (NAO) (Hurrell, 1995). The tripole  
80 pattern of SST over the North Atlantic associated with the winter NAO (see e.g., Visbeck et al., 1998) can  
81 persist during spring and impact the summer circulation over Eurasia (Gastineau and Frankignoul, 2015; Osso et  
82 al., 2018). During summer months, two dominant modes of variability are the summer NAO (Folland et al.,  
83 2009) and the Summer East Atlantic (SEA) pattern (Osso et al., 2018; Osso et al., 2020). During the period  
84 1948-2016, for the summer months of June-September, NAO explained about 36% of variance, while SEA  
85 explained about 16% of variance of sea level pressure (Osborne et al., 2020). A few studies have shown that  
86 such variability of SST and circulation over the North Atlantic has the potential to influence the SWM  
87 circulations over South Asia. For example, the SST anomalies associated with the Atlantic Multidecadal  
88 Oscillations can influence the tropospheric temperature leading to strengthening or weakening of the monsoon  
89 via modulation of the frequency and strength of NAO (Goswami et al., 2006). The cold (positive) phases of the  
90 SST tripole over the North Atlantic have induced stronger westerlies over the northern IO (Krishnamurthy and  
91 Krishnamurthy, 2015). The influences of the extra-tropical North Atlantic/Pacific SST on the South Asian  
92 monsoon are stronger during weak El Nino/La Nina years (Chattopadhyay et al., 2015).

93 In the above backdrop, we examine how changes in the spatial pattern of ocean warming during 2001-2018 have  
94 led to increased dependence of South Asian dust on the North Atlantic Ocean, shifting from the previously  
95 dominant influence of the equatorial Pacific SST. Using observations and reanalysis data we explore the  
96 physical mechanism by which a remote response of the circulation over South Asia is invoked by SST  
97 anomalies over the North Atlantic. We have further performed control and sensitivity studies using an earth  
98 system model to investigate in detail how dust emission and transport is impacted by perturbing SST over the  
99 North Atlantic Ocean. For this study, we have chosen a domain encompassing 65°E-82°E longitude and 24°N-  
100 32°N latitude. We consider this as the dust belt of South Asia. The region is influenced predominantly by SWM  
101 precipitation. Unless stated otherwise, all analyses involving spatial averaging focus only on this region.

102

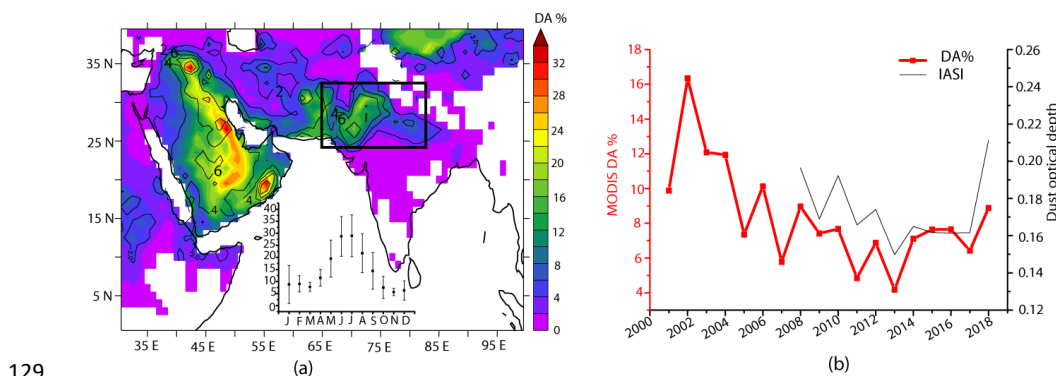
## 103 **2 Data and Models**

### 104 **2.1 Satellite observation and reanalysis data**

105 The main source of dust aerosol data for this study is from the Moderate Resolution Imaging Spectroradiometer  
106 (MODIS) aboard Terra (2001-2018) and Aqua (2003-2018) satellites, which provide the longest satellite-based  
107 information on both aerosol load and size distribution over land and ocean. We have calculated frequency of  
108 days in a year when substantial dust activity is experienced over South Asia ( $DA_{\%}$ ) using MODIS level 3  
109 version 6.1 daily deep blue aerosol optical depth ( $\tau$ ) and Angstrom exponent ( $\alpha$ ). The deep blue algorithm of  
110 MODIS is used to retrieve aerosol information over bright surfaces, like arid regions, where surface reflectance  
111 is low at the blue end of the spectrum (Hsu et al., 2004; Hsu et al., 2006). The criteria used for estimating  $DA_{\%}$



112 are (i)  $\tau > 0.6$  and (ii)  $\alpha < 0.2$  to isolate the days dominated by moderately high load of coarse-mode aerosols.  
113 This yields a map of the main dust source regions in and around South Asia at  $1^\circ \times 1^\circ$  horizontal resolution.  
114 Previously, along with deep blue  $\tau$  and  $\alpha$ , single scattering albedo has also been used to account for the  
115 absorptive property of dust when deriving dust optical depth (Ginoux et al., 2012; Pu and Ginoux, 2018). For  
116 our present purpose,  $\tau$  and  $\alpha$  combination is sufficient since we are deriving frequency of days of dust activity  
117 and not the absolute optical depth. Fig. 1a shows the spatial distribution of  $DA_{\%}$  averaged for 2001-2018 and its  
118 standard deviation (SD). High values of  $DA_{\%}$  coincide with known locations of dust source regions. The SD is  
119 low indicating that high dust activities persist over these regions. The inset in Fig. 1a shows the monthly  
120 climatology of  $DA_{\%}$  with the SD, which reveals that highest values occur during June-July and lowest values  
121 during November. Over the dust belt of South Asia, for 2001-2018, average  $DA_{\%}$  from MODIS Terra is 5.2 (SD  
122 is 1.7) and from MODIS Aqua is 4.2 (SD is 1.7). Changing the threshold values of both  $\tau$  and  $\alpha$  by 50% and  
123 recalculation of  $DA_{\%}$  does not lead to any significant changes in these results. MODIS-derived  $DA_{\%}$  matches  
124 well with year-to-year variability of dust optical depth ( $\tau_d$ ) from Infrared Atmospheric Sounder Interferometer  
125 (IASI) aboard Metop-A (2008-2018) with a correlation coefficient of 0.73, which is significant at 99%  
126 confidence level (Fig. 1b). IASI reports  $\tau_d$  at  $10 \mu\text{m}$  wavelength and at a spatial resolution of  $0.5^\circ \times 0.5^\circ$  (Capelle  
127 et al., 2018). For 2008-2018, IASI dataset yields annual average  $\tau_d$  value of 0.17 (SD of 0.02). In subsequent  
128 analysis, we use combined  $DA_{\%}$  obtained from MODIS Terra and Aqua.



129  
130 **Figure 1: (a) Shading shows spatial distribution of  $DA_{\%}$ , averaged for 2001-2018 and contours are the standard**  
131 **deviations of  $DA_{\%}$  for the same period. The black rectangle indicates the dust belt of South Asia ( $65^\circ\text{E}$ - $82^\circ\text{E}$ ,  $24^\circ\text{N}$ -**  
132  **$32^\circ\text{N}$ ) which is used for subsequent analysis. The monthly climatology and the standard deviation of  $DA_{\%}$  over dust**  
133 **belt of South Asia are shown by black squares and vertical bars respectively in the inset. (b) Time-series of MODIS-**  
134 **derived  $DA_{\%}$  and IASI-retrieved annual dust optical depth over South Asia.**

135

136 To examine the linkages between the spatial variability of SST during different periods and South Asian dust  
137 activity, we have used 3 SST datasets: (1) National Oceanic and Atmospheric Administration (NOAA)  
138 Extended Reconstructed SST (ERSST) version 5 (Huang et al., 2017) available at  $2^\circ \times 2^\circ$  spatial resolution, (2)  
139 Centennial in situ Observation-Based Estimates (COBE) version 2 SST data at  $1^\circ \times 1^\circ$  spatial resolution  
140 (Hirahara et al., 2014) and (3) Optimally Interpolated SST version 2 (OISST) data at  $1^\circ \times 1^\circ$  spatial resolution



141 (Reynolds et al., 2002). All the SST datasets are at monthly temporal resolution. The ERSST version 5 data  
142 combines ship and buoy SST from International Comprehensive Ocean and Atmosphere Dataset (ICOADS)  
143 along with Argo data since 2000. COBE also uses ICOADS data along with data from Kobe collection. Finally,  
144 OISST combines Advanced Very High Resolution Radiometer (AVHRR) retrievals with ship-borne and buoy  
145 data. Atmospheric data such as wind vectors, geopotential height, sea level pressure and velocity potential have  
146 been taken from National Centers for Environmental Prediction/ National Center for Atmospheric Research  
147 (NCEP/NCAR) Reanalysis at  $2.5^{\circ} \times 2.5^{\circ}$  spatial resolution (Kalnay et al., 1996). For precipitation we have used  
148 monthly Global Precipitation Climatology Project (GPCP) version 2.3 data available at  $2.5^{\circ} \times 2.5^{\circ}$  spatial  
149 resolution, which combines rain gauge measurements with satellite observations (Huffman et al., 1997).  
150 Additionally, monthly precipitation data averaged from daily data has been obtained from Precipitation  
151 Estimation from Remotely Sensed Information using Artificial Neural Networks (PERSIANN) at  $0.25^{\circ} \times 0.25^{\circ}$   
152 spatial resolution. PERSIANN algorithm is applied on Gridded Satellite (GridSat-B1) brightness temperature  
153 observation in the infrared region (Ashouri et al., 2015). The precipitation data are then corrected for bias  
154 against GPCP precipitation estimates. To track the large-scale variability over North Atlantic, Hurrell's station-  
155 based seasonal NAO index has been used for the years 2001-2018 (Hurrell, 1995; Hurrell and Deser, 2009).  
156 NAO index is calculated based on the difference between normalized sea level pressure over Lisbon, Portugal  
157 and Stykkisholmur/Reykjavik, Iceland.

## 158 2.2 CESM experiments

159 Simulations were carried out using the Community Earth System Model (CESM) version 1.2 to examine the  
160 mechanism by which SST anomalies over the North Atlantic Ocean impact dust cycle over South Asia. CESM  
161 is a fully coupled model used for simulations of global climate across different spatial and temporal scales.  
162 There are several components to CESM model (example atmosphere, land, sea ice, ocean etc.), which are linked  
163 through a coupler. We have used Community Atmosphere Model version 4 with the Bulk Aerosol Module  
164 (CAM4-BAM) coupled with Community Land Model version 4 in "Satellite Phenology" (CLM-SP)  
165 configuration. Simulations are carried out for trace gases levels corresponding to the year 2000 at  $0.9^{\circ} \times 1.25^{\circ}$   
166 spatial resolution with 26 levels in the vertical.

167 Emission of dust is calculated within CLM model, while dust transport and deposition as well as the radiative  
168 effects are calculated within CAM model (Mahowald et al., 2006). Dust emission follows the treatment of Dust  
169 Entrainment and Deposition scheme of Zender et al. (2003a). Dust emission is based on saltation process, which  
170 depends on modelled wind friction velocity, soil moisture, vegetation and snow cover. This saltation flux occurs  
171 whenever wind friction velocity exceeds a threshold (Marticorena and Bergametti, 1995). Additionally, dust  
172 emission is corrected by a geomorphic source function, which accounts for the spatial variability of erodible  
173 materials (Zender et al., 2003b). In CAM4-BAM dust is emitted in 4 size bins: 0.1-1.0, 1.0-2.5, 2.5-5.0 and 5.0-  
174 10.0  $\mu\text{m}$ . Dust is transported based on CAM4 tracer advection scheme and is removed via dry (gravitational and  
175 turbulent deposition) and wet depositions (convective and large-scale precipitation) (Zender et al., 2003a; Neale  
176 et al., 2010). The solubility factor and scavenging coefficient are taken here as 0.15 and 0.1 respectively.

177 Two sets of simulations have been carried out with CESM: (1) the "Ctrl" simulation, where the atmosphere was  
178 forced with prescribed climatological monthly SST and sea ice from Hadley Centre (1870-1981) and NOAA



179 Optimal Interpolation SST (1981-2010) (Hurrell et al., 2008), and (2) the “NAtl” simulation, where the month-  
180 by-month observed trend in SST during 2011-2018 were imposed over the climatological SST only over the  
181 North Atlantic Ocean. Over rest of the domain climatological SST from Hurrell was prescribed. Thus, the  
182 differences between “NAtl” and “Ctrl” simulations reflect solely the impact of North Atlantic SST anomalies, as  
183 observed during 2011-2018, on atmospheric circulation and dust load. A total of 15 years of simulations have  
184 been carried out for each of Ctrl and NAtl cases with each year being initialized from the atmospheric state at  
185 the end of the previous year. For this study, monthly mean values for the last 10 years of model runs have been  
186 used for both the cases. We have compared  $\tau_d$  from Ctrl run with IASI-retrieved  $\tau_d$  and coarse mode  $\tau$  data  
187 from Aerosol Robotic Network (AERONET) stations at Kanpur (2001-2018), Lahore (2010-2016) and Jaipur  
188 (2010-2017). For this, we have used version 3 AERONET level 2.0 cloud cleared aerosol data.

189

### 190 **3 Results and discussion**

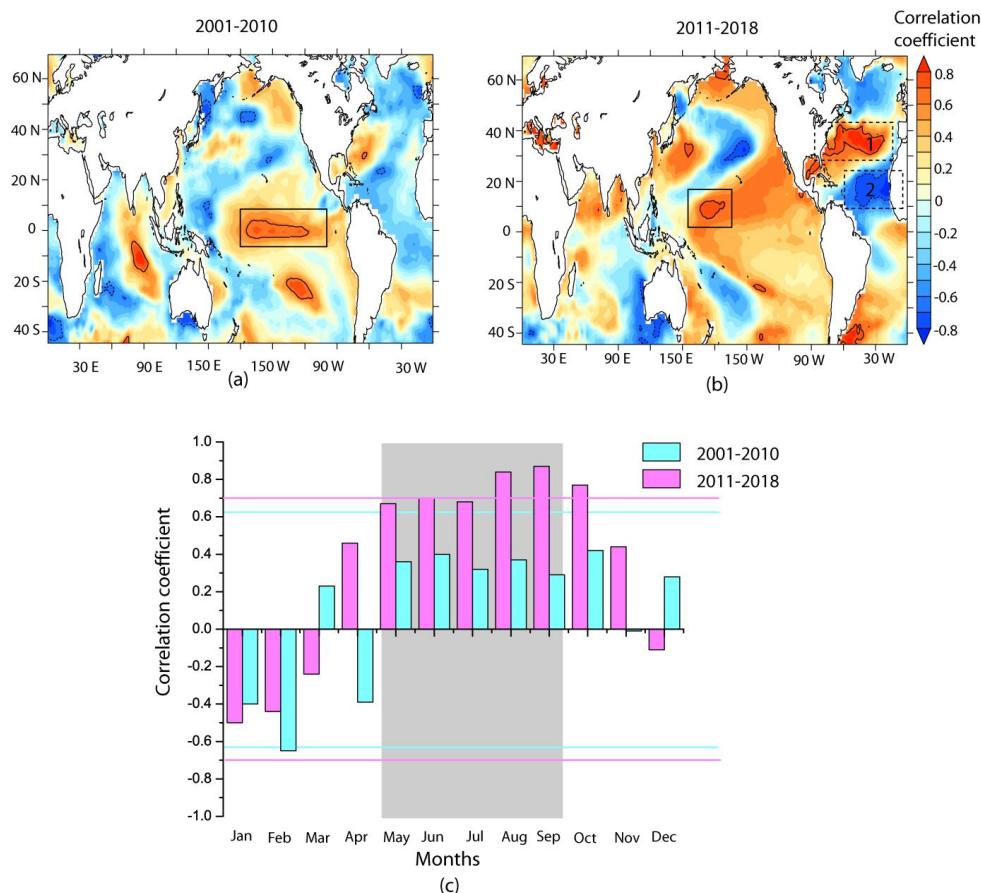
191 We first demonstrate that there is a change in the relation between dust aerosol variability over South Asia and  
192 global SSTs during 2001-2018 with the role of the North Atlantic Ocean assuming importance in the recent  
193 years. We next discuss the possible physical mechanism involved by which SST anomalies over key regions in  
194 the North Atlantic influence the circulation over South Asia. Finally, CESM simulation results are used to  
195 isolate the effect of North Atlantic SST variability on dust emission and transport over South Asia.

#### 196 **3.1 Decadal change in correlation between dust and SST**

197 We have carried out correlation analysis of  $DA_{\%}$  over the dust belt of South Asia with annual averaged SSTs  
198 separately for the periods 2001-2010 and 2011-2018. These are the two periods when the signature of shift from  
199 the Pacific to the Atlantic SST modulation of  $DA_{\%}$  is the strongest. The maps showing spatial distribution of the  
200 correlation coefficients for these two periods are shown, respectively, in Figures 2a and b. During 2001-2010,  
201 the largest coherent region with which  $DA_{\%}$  shows significant positive correlation encompasses central  
202 equatorial Pacific (Fig. 2a; marked by continuous rectangle). During 2011-2018 this region has contracted and  
203 shifted north-eastwards (Fig. 2b; continuous rectangle), while two new regions of significant correlations have  
204 emerged: (1) over mid-latitude North Atlantic centered on 40°N latitude (significant positive correlation) and (2)  
205 over sub-tropical North Atlantic centered on 20°N latitude off the western coast of North Africa (significant  
206 negative correlation). These two regions are shown by dashed rectangles and are marked as “1” and “2”  
207 respectively in Fig. 2b. Though a weak signature of this correlation pattern is present in 2001-2010, it has  
208 emerged significantly strong during 2011-2018. Conducting month-by-month analysis of the impact of SST on  
209  $DA_{\%}$  (not shown) it is seen that the positive correlation between  $DA_{\%}$  and SST over central equatorial Pacific  
210 during 2001-2010 is most prominent during September-October; while that over the North Atlantic during 2011-  
211 2018 is most prominent during April-June, which are used here for subsequent analysis. We have constructed a  
212 North Atlantic Difference Index (NADI) of SST by taking into account the regions where  $DA_{\%}$  have significant  
213 correlation with the North Atlantic SST as seen in Fig. 2b. NADI is the standardised difference in SST over  
214 mid-latitude (Region 1, taken as 70°W-25°W longitude, 25°N-40°N latitude) and sub-tropical (Region 2, taken  
215 as 70°W-25°W longitude, 10°N-20°N latitude) North Atlantic, averaged for April-June. Fig. 2c depicts the



216 variation of correlation coefficient between April-June NADI and monthly  $DA_{\%}$  over South Asia separately for  
217 2001-2010 and 2011-2018. Monthly  $DA_{\%}$  is simply the percentage of days in a month when  $\tau > 0.6$  and  $\alpha < 0.2$ .  
218 Fig. 2c clearly shows that the correlation between NADI and  $DA_{\%}$  is stronger and significant (at 95% confidence  
219 level) for 2011-2018, during May-October, in comparison to 2001-2010. These months having significant  
220 correlation largely coincide with the high dust months over South Asia, where dust loads peak during May-June.  
221 During 2011-2018, conducting partial correlation analysis between April-June NADI and annual  $DA_{\%}$  adjusted  
222 for the central equatorial Pacific SST (taken as 178°W-100°W, 10°S-10°N) improves the correlation to 0.93,  
223 which is significant at 99% confidence level. At the same time, partial correlation between the central equatorial  
224 Pacific SST and  $DA_{\%}$  adjusted for NADI gives a correlation coefficient of -0.36, which is not significant. For  
225 2001-2010, a significant negative relation between NADI and  $DA_{\%}$  is seen only for the month of February.



226  
227 **Figure 2: Correlation between percentage frequency of annual dust activity ( $DA_{\%}$ ) and annual average SST for (a)**  
228 **2001-2010 and (b) 2011-2018. The black contours enclose the regions where correlation coefficient is significant at**  
229 **95% confidence level. The continuous (dashed) boxes show the main regions with which  $DA_{\%}$  over South Asia have**  
230 **significant correlations over the Pacific (Atlantic) Ocean (see text for details). In (b) the regions used for constructing**  
231 **the North Atlantic Difference Index (NADI) are marked as “1” and “2”. (c) Correlation between April-June NADI**  
232 **and monthly  $DA_{\%}$  are plotted. The blue and pink horizontal lines indicate the 95% confidence levels for 2001-2010**



233 and 2011-2018 respectively. The grey shaded region highlights the months which have  $DA_{\%}$  values greater than  
234 annual average  $DA_{\%}$ .

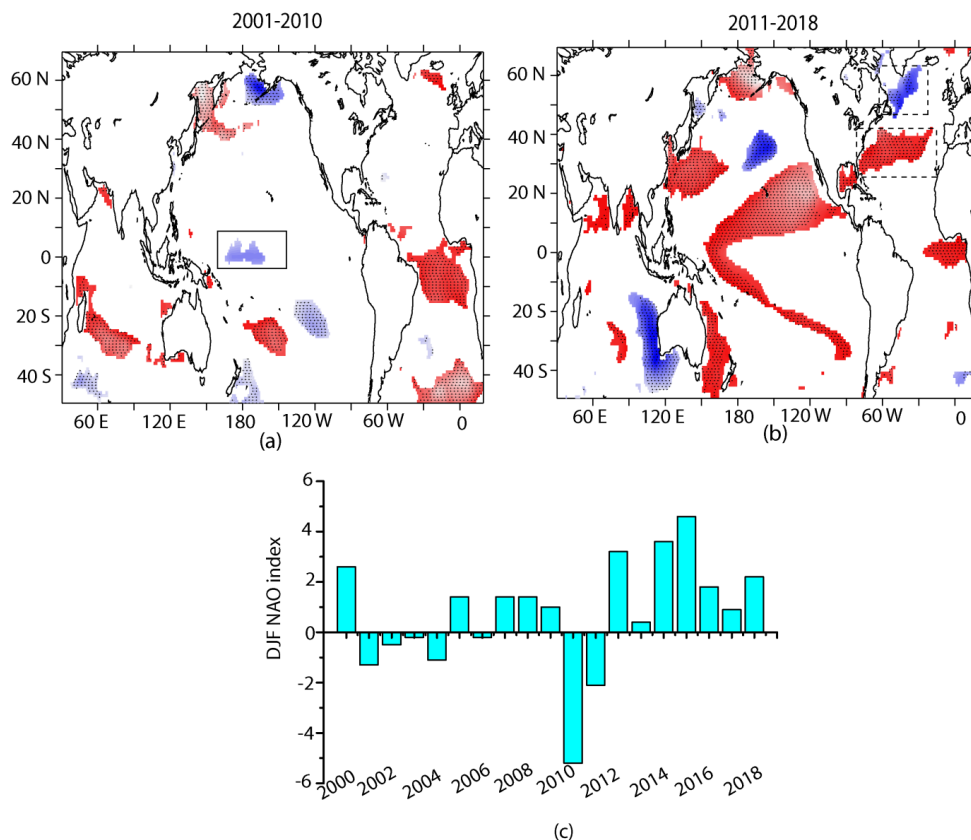
235

236 The central equatorial Pacific, where the SST is significantly correlated with  $DA_{\%}$  during 2001-2010, is  
237 historically a prime region driving the variability of the SWM; and by some extension, dust emission and  
238 transport. Several studies have shown that warming of the central equatorial Pacific SST leads to drought over  
239 South Asia by inducing an anomalous descending motion (e.g., Kumar et al., 2006; Rajeevan and Pai, 2007).  
240 Since the 1990s, stronger El Nino signals have been detected in the central Pacific SST compared to the eastern  
241 Pacific (Yeh et al., 2009; Lee and McPhaden, 2010). Interestingly, there has been a cooling trend in the central  
242 Pacific SST during 2001-2010 (of  $-0.8^{\circ}\text{C decade}^{-1}$ ) when this region was a major driver of  $DA_{\%}$  over South Asia  
243 (continuous box in Fig.3a). This formed a part of the hiatus within the ongoing global warming trend since the  
244 beginning of the 21<sup>st</sup> century, leading to a slowdown in global mean surface temperature warming rate to 0.02-  
245 0.09 $^{\circ}\text{C}$  (Xie and Kosaka, 2017). Several studies have shown that this has coincided with the negative phase of  
246 the Pacific Decadal Oscillation and has been largely attributed to the internal variability over the Pacific Ocean  
247 (Kosaka and Xie, 2013, 2016; Trenberth and Fasullo, 2013; England et al., 2014). The extreme El Nino of 2015  
248 brought about the end of the global warming hiatus (Hu and Fedorov, 2017). This cooling trend is more  
249 prominent during the boreal winter months (Trenberth et al., 2014).

250 With the end of the global warming hiatus, the North Atlantic Ocean emerged as an important driver of the  
251 interannual variability of  $DA_{\%}$  over South Asia during 2011-2018. A few recent studies have shown that since  
252 late 1970s the Atlantic Ocean has assumed increasing influence over the climate of the Asian monsoon region as  
253 the influence of the tropical Pacific has reduced (Kucharski et al., 2007; Sabeerali et al., 2019; Srivastava et al.,  
254 2019). This in-turn impacts the circulation responsible for dust uplift and transport. The spatial pattern of  
255 correlation between  $DA_{\%}$  and SST for 2011-2018 in Fig. 2b shows resemblance to SST tripole pattern  
256 associated with the positive phase of NAO (Bjerkness, 1964; Visbeck et al., 2001; Rodwell et al., 1999; Han et  
257 al., 2016). In general, the positive phase of NAO projects to positive SST anomaly over the mid-latitude North  
258 Atlantic and negative SST anomalies over the sub-tropical and the sub-polar North Atlantic (also see  
259 Supplementary Fig. S1 a-c).  $DA_{\%}$  is significantly correlated with the mid-latitude (Region 1 in Fig. 2b) and sub-  
260 tropical (Region 2 in Fig. 2b) arms of the SST tripole. This tripole have recently changed sign from being  
261 negative (warm phase) during 2001-2010 to positive (cold phase) during 2011-2018 (Supplementary Fig. S1 d-  
262 e). That is, during 2011-2018, SST over North Atlantic shows a decreasing trend in the sub-tropics (centered on  
263 20 $^{\circ}\text{N}$  latitude), which is not significant, a significant (at 95% confidence level) increasing trend over the mid-  
264 latitude (centered on 40 $^{\circ}\text{N}$  latitude) and again a significant decreasing trend in the subpolar region (centered on  
265 60 $^{\circ}\text{N}$  latitude, dashed boxes in Fig. 3b). The SST trends over the North Atlantic during 2001-2010, on the other  
266 hand, are not significant. In fact, December-February NAO index was neutral to negative during 2001-2010  
267 (average NAO index -0.4) and changed to positive during 2011-2018 (average NAO index 2.4) (Delworth et al.,  
268 2016; Iles and Hegerl, 2017) in tune with the switch in the sign of SST tripole during this period (Fig. 3c). Thus,  
269 to sum up, with the resumption of global warming, the North Atlantic SST seems to assume importance in  
270 controlling dust activity over South Asia, indicating a shift from the well-known importance of the Pacific SST.  
271 The linkage is through a persistent positive phase of NAO during 2011-2018 and its imprint on the North



272 Atlantic SST tripole, the latter being in its positive (cold) phase during this period. In the next section we  
273 discuss the physical mechanism responsible for North Atlantic SST leading to increased South Asian dust  
274 activity.



275

276 **Figure 3: Regions experiencing positive (red shades) and negative (blue shades) trends in sea surface temperature**  
277 **during (a) September-October of 2001-2010 and (b) April-June of 2011-2018 significant at 90% confidence level. The**  
278 **overlaid black stippling shows the regions where the trend is significant at 95% confidence level. (c) Time series of**  
279 **December-February Hurrell's station-based NAO index for 2000-2018.**

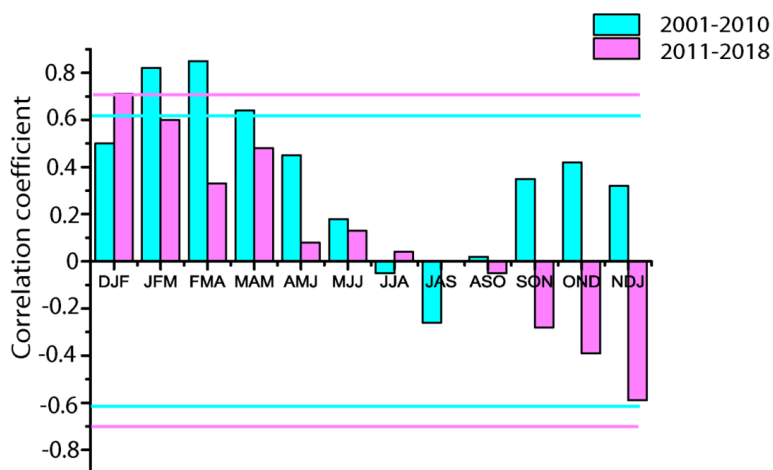
280

### 281 3.2 Physical Mechanism linking South Asian dust with Atlantic SST

282 The above observations invoke the question: what could be the possible mechanism by which the changes in  
283 North Atlantic SST impact South Asian dust activity during 2011-2018, when the Pacific Ocean influence has  
284 reduced? The 'April to June North Atlantic Difference Index' (NADI, described in Section 3.1) is more strongly  
285 and persistently correlated to winter and spring NAO index during 2001-2010 than during 2011-2018 (Fig. 4).  
286 This indicates that the relation between winter and spring NAO and NADI (via SST tripole) has changed during  
287 2011-2018, which has impacted circulation over South Asia and, thereby, dust load. To understand the  
288 mechanism involved, we have estimated the correlation between April-June NADI and different meteorological



289 fields averaged for the months May-September when NADI is significantly correlated with  $DA_{50}$  (see Fig. 2c)  
290 and also when high dust activity is widespread over South Asia. The results in Fig. 5 reveal that during 2001-  
291 2010, NADI projects on to a cyclonic circulation anomaly at 850-700 hPa pressure level northwest off the  
292 British Isles (red box in Fig. 5a) and a tripole-like SST anomaly with warming in the Norwegian Sea (Fig. 5b).  
293 This resembles the Summertime East Atlantic (SEA) pattern, which is the second dominant mode of variability  
294 after NAO over the North Atlantic Ocean during summer (Wulff et al., 2017; Osso et al., 2018; Osborne et al.,  
295 2020), although, there are certain differences: (1) the cold sub-polar arm of the SST tripole has greater  
296 southward extension (Fig.5b) and (2) an additional positive sea level pressure anomaly along western North  
297 Atlantic between 10°N-50°N latitude is detected (Fig. 5c). Velocity potential at 850 hPa pressure level (green  
298 contours in Fig. 5c) during May-September of 2001-2010 points to large-scale descending motion and  
299 divergence over the North Atlantic. This is associated with negative precipitation anomalies over the cooler SST  
300 regions of the North Atlantic, as well as, over Sahel (green contours in Fig.5b). The impact of NADI over South  
301 Asia is mostly felt through the reduction in precipitation over west India and westerly anomalies in the south-  
302 central Indo-Gangetic plain. Negative precipitation anomalies are also present over the dust source regions of  
303 the Middle East and southern part of Central Asia.



304

305 **Figure 4: Correlation between seasonal NAO index and April-June North Atlantic Difference Index (NADI)**  
306 **separately for 2001-2010 and 2011-2018. The blue and pink horizontal lines indicate the 95% confidence levels for**  
307 **2001-2010 and 2011-2018 respectively.**

308

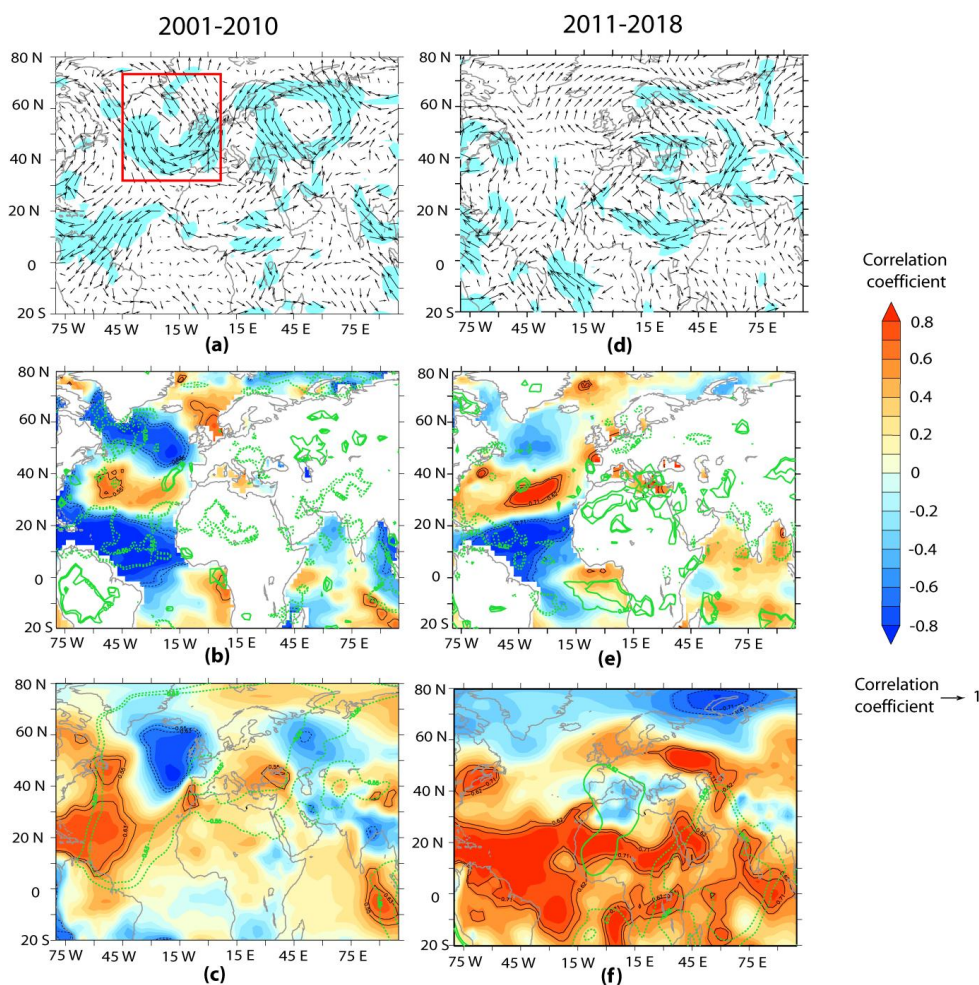
309 During 2011-2018, the significant imprint of NADI on SEA wind pattern northwest off the British Isles is  
310 absent (Fig. 5d), implying a shift in the relation between them. With the North Atlantic SST tripole changing  
311 sign from warm during 2001-2010 to cold during 2011-2018 (Supplementary Fig. S1 d-e), NADI is significantly  
312 correlated with the mid-latitude and sub-tropical arms of the SST tripole, but not with the sub-polar arm of the  
313 SST tripole (shading in Fig. 5e). Additionally, there is an eastward shift in the region of positive correlation  
314 between NADI and the mid-latitude arm of the tripole and a southward shift in the region of negative correlation



315 between NADI and the sub-tropical arm of the tripole. The region of low pressure off the British Isles, seen  
316 during 2001-2010, is absent during 2011-2018 (Fig. 5f) due to the absence of the SEA pattern. Instead,  
317 associated with the cooling of sub-tropical North Atlantic SST, a large region of positive correlation between  
318 NADI and sea level pressure over the sub-tropical North Atlantic appears (Fig. 5f). These changes in relation  
319 between NADI and the North Atlantic SST tripole have resulted in convergence, as indicated by 850 hPa  
320 velocity potential (green contours in Fig. 5f), and positive precipitation anomaly over the Mediterranean region  
321 including North Africa and northwestern part of the Arabian Peninsula (green contours in Fig. 5e). The  
322 summertime wet anomaly over the Mediterranean region leads to anomalous descending motion over South  
323 Asia, Middle East and East Africa, which is indicated by negative velocity potential at 850 hPa over this region  
324 (Fig. 5f). The net effect is that the region of positive sea level pressure anomalies linked with the cooler sub-  
325 tropical arm of the SST tripole now stretches to encompass the Sahel, Middle East, western India and the central  
326 part of northern IO (orange shading in Fig. 5f). Over South Asia this development suppresses precipitation over  
327 different regions of India and leads to general dryness. More importantly, as seen by the vectors in Fig. 5d, the  
328 positive sea level pressure anomaly over the Middle East invigorates the westerlies carrying dust from  
329 Southwest Asia to South Asia. The northerlies which are important for dusty weather over Pakistan-  
330 Afghanistan-Iran are also strengthened.

331 In summary, although persistent positive phase of NAO prevailed during 2011-2018, a disassociation between  
332 NAO and NADI influenced circulation over the Eurasian sector and over North Africa. Over South Asia and  
333 surroundings, this projected to increased subsidence and positive anomalies of sea level pressure, which resulted  
334 in general weakening of the monsoon and strengthening of the dust-transporting northerlies and westerlies.

335



336

337 **Figure 5:** Correlation between the April-June North Atlantic Difference Index (NADI) and different meteorological  
 338 parameters from NCEP/NCAR Reanalysis averaged for May-September for (left panels) 2001-2010 and for (right  
 339 panels) 2011-2018. (a) and (d) Arrows show correlation between NADI and wind vectors averaged between 850 and  
 340 700 hPa pressure levels. Light blue shade highlights the regions where one of the components of the wind vector is  
 341 significantly (95% confidence level) correlated with NADI. (b) and (e) Shading shows correlation between NADI and  
 342 SST and the green contours enclose the regions where significant correlation exists between NADI and precipitation.  
 343 Black contours indicate the regions where correlation between NADI and SST are significant. (c) and (f) Shading  
 344 shows correlation between NADI and sea level pressure and the green contours enclose the regions where significant  
 345 correlation exists between NADI and velocity potential at 850 hPa pressure level. Black contours indicate the regions  
 346 where correlation between NADI and sea level pressure are significant. For all the panels continuous and dashed  
 347 contours are indicative of significant positive and negative correlations respectively; inner and outer contours of a  
 348 particular colour indicate 95% and 90% confidence levels respectively.

349

350

351

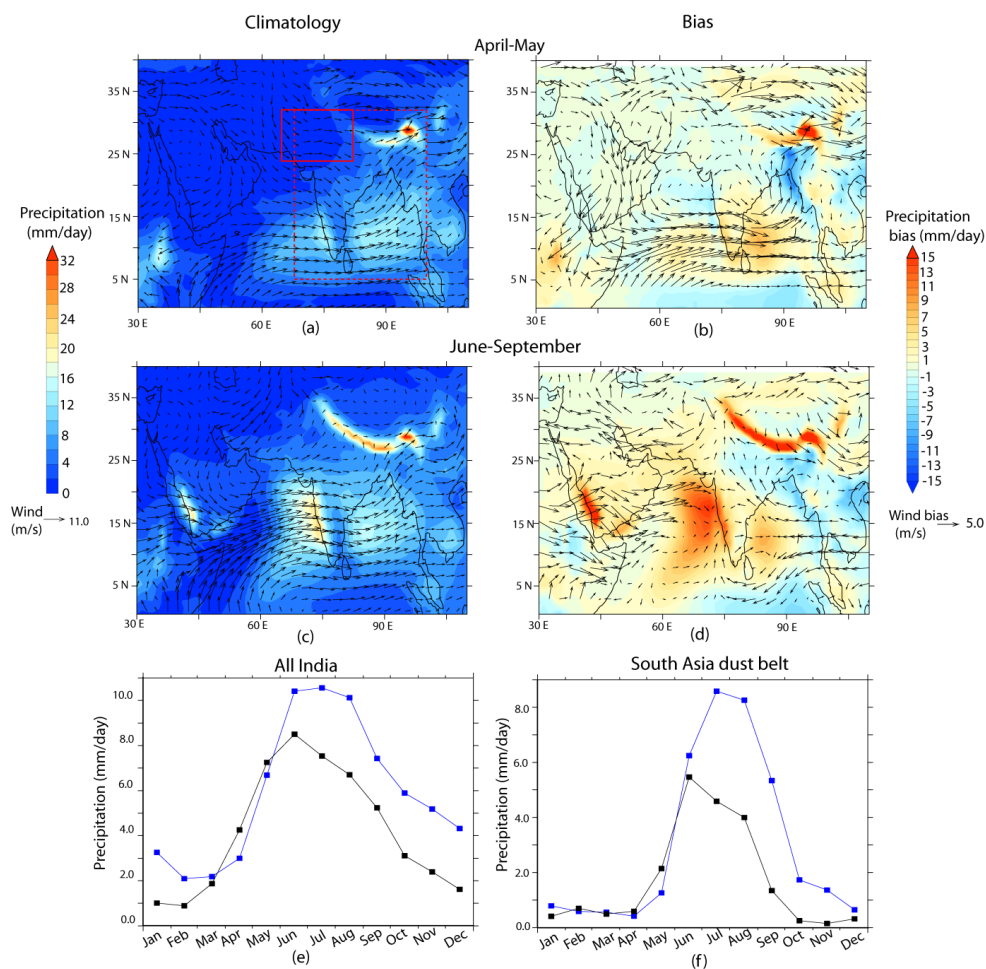


### 352 3.3 CESM simulation of Atlantic Ocean influence

353 The teleconnection between the North Atlantic SST and dust load over South Asia is explored further with the  
354 help of CESM simulations, with a view to isolate the contributions from North Atlantic SST anomalies. To  
355 achieve this, we have compared two sets of simulations, as explained in Section 2.2, for ten model years: one  
356 with climatological SST (Ctrl run) and the other with the SST trend for 2011-2018 superposed on the  
357 climatological SST over the North Atlantic (NAtl run). The difference (NAtl – Ctrl runs) yields the contribution  
358 solely from North Atlantic SST anomalies. It is important to note here that while NADI reflects the gradient  
359 between the mid-latitude and sub-tropical branches of North Atlantic SST, SST anomalies imposed for the NAtl  
360 run illustrate the response due to spatial pattern of SST anomalies over the entire North Atlantic due to  
361 persistent positive phase of NAO.

362 In general, CESM simulations can reproduce the main features of the North Atlantic summer climate and  
363 circulation, on which we are focussed here. Sea level pressure-based empirical orthogonal analysis carried out  
364 for CESM Large Ensemble simulations for 1920-2012 have revealed that NAO accounts for 40-member mean  
365 variance of 43% for winter months (Deser et al., 2017b). With our ten years CESM simulation we can still  
366 identify the dominant modes of variability. Empirical orthogonal function using June-September sea level  
367 pressure from CESM shows that NAO accounts for 63% and SEA pattern accounts for 14% of sea level  
368 pressure variances (Supplementary Fig. S2). To examine CESM performance over South Asia we have  
369 compared outputs from CESM Ctrl simulation with NCEP/NCAR wind at 850 hPa pressure level and  
370 PERSIANN precipitation separately for the spring inter-monsoon (April-May) and SWM (June-September)  
371 periods in Figs. 6 a-d. The comparisons reveal that the Ctrl run reproduces the main features of circulations and  
372 precipitation over South Asia fairly well, although with certain biases, which impact dust distribution and its  
373 temporal evolution. During April-May anomalous westerlies drive positive precipitation bias over peninsular  
374 India and southeast Bay of Bengal (Figs. 6 a and b). The anomalous southerlies over the southern part of the  
375 Indo-Gangetic plain lead to negative precipitation bias there, but a positive bias over the eastern Himalayas.  
376 During June-September, there are positive biases of precipitation along the west coast of India, southern India,  
377 the Himalayan foothills and most of the Middle East. Negative bias in precipitation prevails over eastern India  
378 and Southeast Asia bordering northeastern Bay of Bengal (Figs. 6 c and d). The positive bias along the west  
379 coast of India is associated with stronger westerlies in the Ctrl run. The anomalous anticyclone over the northern  
380 Bay of Bengal leads to a comparatively lower magnitude negative bias in precipitation of around 30%. This  
381 dipole in precipitation bias over the South Asian monsoon region has been recognized in Coupled Model  
382 Intercomparison Project Phase 5 (CMIP5) suite of models (Sperber et al., 2013) and has been attributed to  
383 several causes: SST bias over western equatorial IO (Annamalai et al., 2017); suppression of moist convection  
384 processes due to smoothening of topography (Boos and Hurley, 2013); weak advection of cold-dry air off  
385 Somali coast which reduces available moisture (Hanf and Annamalai, 2020). Comparing temporal evolution of  
386 CESM simulated precipitation with observations from PERSIANN (Figs. 6e and f) we see that generally wet  
387 bias prevails over both Indian domain (Fig. 6e) and the South Asian dust belt (Fig. 6f). CESM simulates one-  
388 month delay in the peak monsoon rainfall over these regions.

389



390

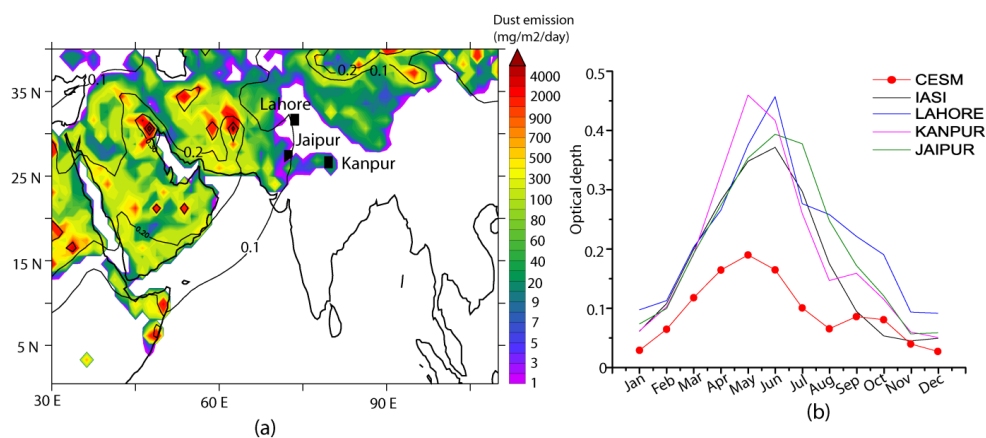
391 **Figure 6: Comparison of CSM-Ctrl simulation with observations/reanalysis data. CSM simulated climatology of**  
 392 **precipitation and wind for (a) April-May and (c) June-September are shown. Differences between CSM simulated**  
 393 **precipitation (shading) with that of PERSIANN and CSM simulated wind (arrows) with that of NCEP/NCAR**  
 394 **reanalysis at 850 hPa pressure level are given for (b) April-May and (d) June-September. Time evolution of CSM**  
 395 **(blue curve) and PERSIANN precipitation (black curve) over (e) All India (5°N-32°N latitude, 68°E-100°E longitude)**  
 396 **and (f) the South Asian dust belt (24°N-32°N latitude, 65°E-82°E). These domains are, respectively, indicated in (a) by**  
 397 **dashed and continuous red boxes.**

398

399 In general, CSM Ctrl reproduces the main dust emission regions over South and Southwest Asia (Fig.7a) along  
 400 with temporal evolution of dust optical depth ( $\tau_d$ , Fig.7b). However, the positive bias in precipitation over dust  
 401 source region, prevailing almost throughout the year, leads to underestimations of  $\tau_d$  compared to observations.  
 402 This discrepancy between CSM and observations is low during the winter months and increases during the  
 403 monsoon months when CSM simulates about  $3.5 \text{ mm day}^{-1}$  positive bias in precipitation over the South Asian  
 404 dust belt and  $\sim 2 \text{ m s}^{-1}$  easterly wind bias. For example, during May when  $\tau_d$  peaks, CSM simulates  $\tau_d$  of  $\sim 0.2$ ,



405 while AERONET coarse mode  $\tau$  over Kanpur, Jaipur and Lahore are almost double. Negative bias in CESM  $\tau_d$   
406 is also apparent when compared to IASI-observed  $10 \mu\text{m}$   $\tau_d$  over South Asia (Fig.7b). Although precipitation  
407 bias during April-May is low ( $\sim 0.1 \text{ mm day}^{-1}$ , Fig. 6b), easterly wind bias of  $0.7 \text{ m s}^{-1}$  leads to low transport  
408 from the west. Similar negative bias in dust associated with weak northwesterlies over the Indo-Gangetic plain  
409 has been noted for CESM-CAM5 simulation submitted to CMIP5 (Sanap et al., 2014). One important reason for  
410 CESM underestimation of  $\tau_d$  can be the exclusion of anthropogenic sources of dust, which contributes to nearly  
411 half of the total annual dust emission (Ginoux et al., 2012). Several improvements in simulating dust with  
412 CESM have been suggested by updating dust emission size distribution, optical properties, wet deposition  
413 parameterizations and tuning soil erodibility (Albani et al., 2014). While further improvements in CESM for  
414 better representation of dust cycle over South Asia is a topic for future, in case of this study, notwithstanding the  
415 negative bias, CESM Ctrl simulation is able to simulate the pattern of spatial distribution and seasonal evolution  
416 of South Asian dust. This is adequate for the present work as we are here interested in the direction of change in  
417 simulated dust load due to the North Atlantic SST tripole rather than on the absolute magnitude of  $\tau_d$ . With this  
418 understanding of the limitations of CESM simulation we proceed to examine the mechanism via which is SST  
419 variability over the North Atlantic is responsible for perturbing dust load over South Asia.



420

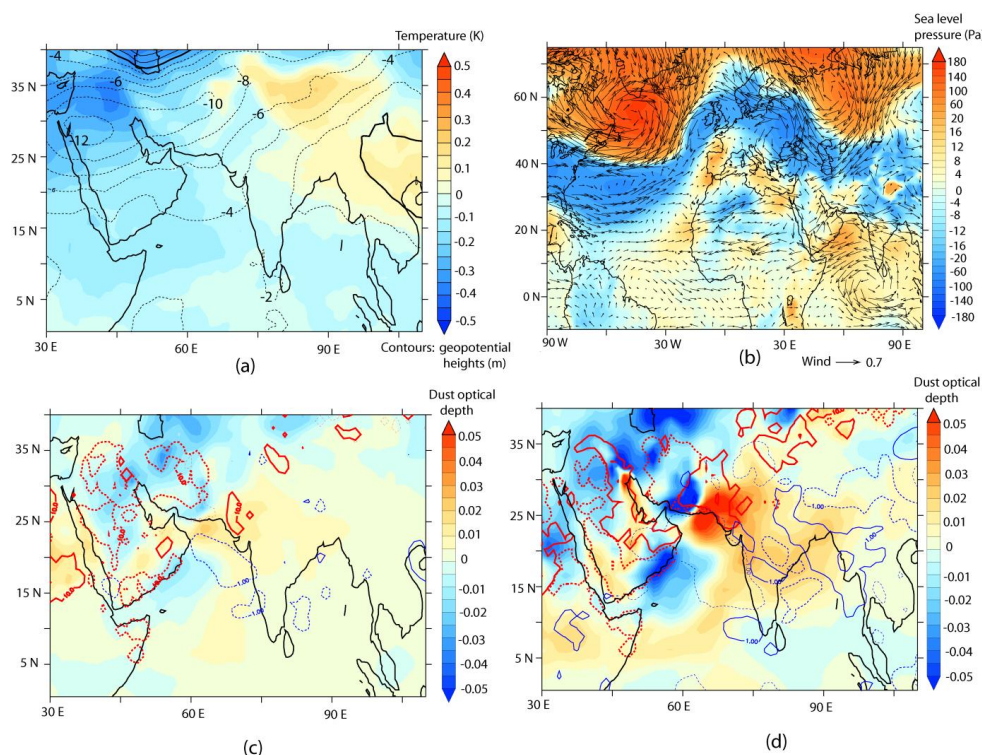
421 **Figure 7: (a) Shading shows the distribution of main dust emitting regions from CESM and the contours indicate**  
422 **dust optical depth. Both of these parameters have been averaged for ten model years. (b) Comparison of monthly**  
423 **climatology of dust optical depth from CESM-Ctrl simulation with IASI and AERONET (Lahore, Kanpur and**  
424 **Jaipur) observations.**

425

426 The differences between NATl and Ctrl simulations for May-September are shown in Fig. 8, which highlights  
427 that the North Atlantic SST anomaly, similar to during 2011-2018, can modulate South Asian dust activity via a  
428 combination of reduced precipitation over the northern IO and strengthening of the dust-bearing northwesterlies  
429 over the dust source regions. Cold SST tripole anomaly results in cooling in the upper troposphere and lowering  
430 of the geopotential heights over South and Southwest Asia; both of which are important indicators of a weak  
431 South Asian monsoon circulation (Fig. 8a). An east-west wave train over the mid-latitude and sub-polar region  
432 of Eurasia sets-in with anticyclonic circulation over the sub-polar and cyclonic circulations over the mid-latitude



433 North Atlantic and also over the British Isles (Fig. 8b). Furthermore, a positive anomaly of sea level pressure  
434 extends eastwards from the sub-tropical North Atlantic and is particularly strong over the northern IO. These  
435 anomalies are similar to the response of the sea level pressure to NADI seen in the tropics; but are opposite to  
436 that seen north of the mid-latitudes (Fig. 5f). Previously, model simulations have shown that the tropical North  
437 Atlantic SST opposes the response of sea level pressure to the extra-tropical part of the cold SST tripole  
438 (Osborne et al., 2020). A cyclonic circulation over the central equatorial IO and an anticyclonic circulation over  
439 the northwestern IO inhibit the inflow of moisture into much of the Indian subcontinent leading to deficit  
440 rainfall. It is the westerlies, which form the northern branch of the anticyclone, that transport dust from the  
441 South Asian sources. For May-September, maximum increase in  $\tau_d$  due to SST tripole is located over the South  
442 Asian dust source region with dust emissions from the Thar being the main contributor (Fig. 8c). While over the  
443 dust source regions the increase in  $\tau_d$  is within 10%, dust transport by the strengthened westerlies can lead up to  
444 20% increase in  $\tau_d$  in the eastern Indo-Gangetic plain. Simultaneously, anomalous southerlies and  
445 southeasterlies over the Arabian Peninsula suppress dust activity in the region (Fig 8b and c). The peak increase  
446 in  $\tau_d$  over South Asia due to North Atlantic SST is observed during June, when ~30% increase in  $\tau_d$  compared  
447 to CESM-simulated climatological values is achieved over the South Asian dust source regions (Fig. 8d). To test  
448 the significance of the positive anomalies of  $\tau_d$ , we carried out Monte Carlo calculations by randomly selecting  
449 6 years from NATl and Ctrl simulations and differencing the  $\tau_d$ . By repeating this procedure 600 times, we find  
450 that in 90% cases NATl-Ctrl yields positive anomalies of  $\tau_d$ . It is important to note that although there is a  
451 rainfall deficit over South Asia and the northern IO, only a small area within the main dust source regions are  
452 impacted. This implies that a general increase in dryness and  $\tau_d$  due to cold phase of North Atlantic SST tripole  
453 is widespread over South Asia. However, the strengthened westerlies are responsible for enhanced dust flux  
454 over the dust belt of South Asia. In this context, it is also worth mentioning that earlier works have reported that  
455 cooling over the North Atlantic, either associated with the cold phase of Atlantic Multidecadal Oscillation or  
456 due to the slowdown of the Atlantic Meridional Oscillation, is associated with weakened monsoon (e.g.,  
457 Goswami et al., 2006; Zhang and Delworth, 2006; Feng and Hu, 2008; Liu et al., 2020). At decadal scale,  
458 rainfall data for 1901-2004 showed that the positive (cold) phase of the SST tripole is associated with excess  
459 monsoon over India due to strengthening of the westerlies over the northern IO (Krishnamurthy and  
460 Krishnamurthy, 2015). However, the sign of correlation between the South Asian monsoon and the SST tripole  
461 has undergone changes since 2000 with the negative (warm) phase of the SST tripole being associated with  
462 strong monsoon over South Asia and vice versa (Gao et al., 2017), implying interdecadal shifts in the relation  
463 between the two. These observations are supportive of our arguments above.



464

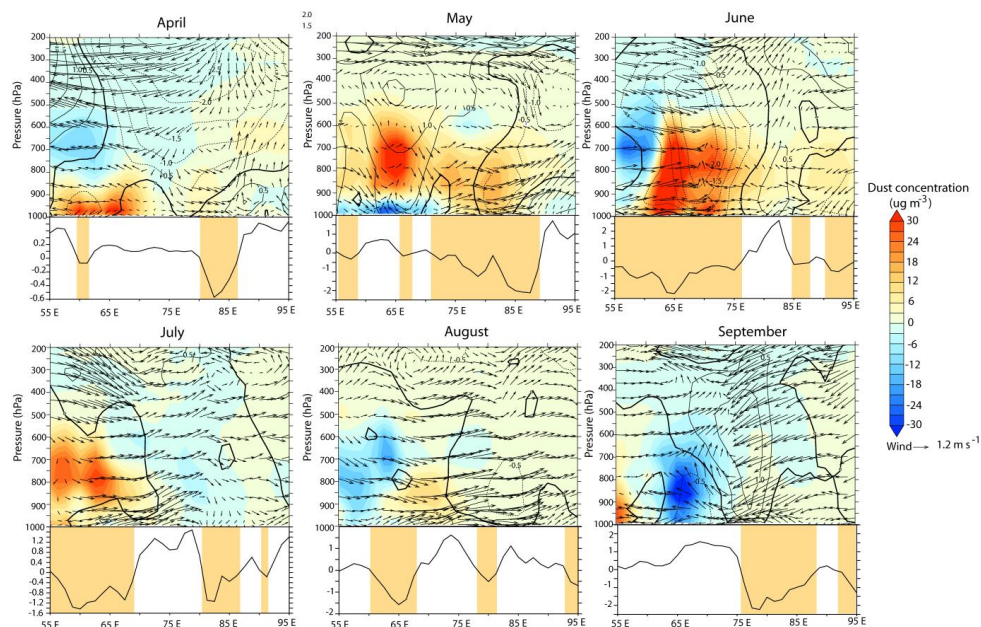
465 **Figure 8: Differences between CSM-NAtl and CSM-Ctrl simulations for (a-c) May-September. (a) Shading and**  
466 **contours indicate differences in temperature and geopotential height respectively at 200 hPa pressure level. (b)**  
467 **Shading indicates difference in sea level pressure and the arrows indicate difference in wind vectors at 850 hPa**  
468 **pressure level. (c) Difference in dust optical depth over the northern Indian Ocean and surrounding regions are**  
469 **shown by shading. The thick red contours enclose the regions where dust emission flux difference is greater than 10**  
470 **mg m<sup>2</sup> day<sup>-1</sup> and the thin blue contours enclose the regions where precipitation difference is greater than 1 mm day<sup>-1</sup>.**  
471 **(d) Same as (c) but for the month of June. For all contours positive values are shown by continuous lines and**  
472 **negative values are shown by dashed lines.**

473

474 The increase in  $\tau_d$  discussed above is enabled by strengthening of dust-transporting westerlies at 800 hPa  
475 pressure level, which can, averaged for May to September, increase dust concentration by 20% at this altitude.  
476 This furthers when we analyse month-by-month changes in dust transport, as shown in Fig. 9, where a much  
477 stronger influence of North Atlantic SST tripole on dust concentrations is evident. The positive anomalies of  
478 dust concentration slowly start to build up during April to reach a peak during June and then subside by  
479 September. During May and June, the North Atlantic SST tripole can enhance dust concentration by 40-50% in  
480 the lower and mid-troposphere over the South Asian dust belt. These are also the months when maximum  
481 negative anomalies of precipitation are seen, following which positive anomalies of precipitation builds up.  
482 During May, maximum dust concentration anomaly centered on 800 hPa pressure level is associated with  
483 transport from the eastern Arabian Peninsula (due to anomalous southwesterly). During June, on the other hand,  
484 the strengthened northerlies transport dust all the way from eastern part of Central Asia into South Asia between  
485 60°-75°E longitudinal belts. Additionally, descending motion above 500 hPa pressure level leads to trapping of



486 dust below this level. The overall weakening of the South Asian monsoon circulation is also demonstrated by  
487 the anomalous upper level westerlies.



488  
489 **Figure 9:** Sections along 25°N latitude illustrating month-wise differences in dust transport between CESM-Natl and  
490 CESM-Ctrl simulations. In upper part of each panel, shadings indicate difference in dust concentrations between the  
491 two simulations, the vectors are the differences in zonal and vertical components of wind and the contours are the  
492 differences in meridional component of wind. Continuous (dashed) contours indicate southerly (northerly) wind  
493 anomalies. The lower part of each panel plots precipitation differences, in mm day<sup>-1</sup>, between CESM-Natl and  
494 CESM-Ctrl simulations along 25°N latitude. The orange shades indicate the longitudinal belts which have negative  
495 anomalies of precipitation. Note that the vertical velocity is expressed as Pa s<sup>-1</sup> and has been multiplied by 40.

496

#### 497 4 Conclusions

498 Our study underlines the need to look at large-scale factors, which are global in nature, in significantly  
499 modulating dust load over South Asia, in addition to changes in local factors. This is specifically relevant  
500 considering the fact that about 50% of dust over this region is transported from remote (non-local) sources  
501 (Banerjee et al., 2019). In this light, we have attempted to understand how changes in large-scale SST patterns  
502 can impact dust emissions and transport pathways in this region. The “memory” of SST provides a bridge  
503 between the circulation changes taking place across the globe. Our study relies on satellite data which are only  
504 available since 2001. Even with this we see significant changes in terms of the relative importance of SST from  
505 different regions driving interannual variability of dust over South Asia.

506 Our study shows that during the second decade of the 21<sup>st</sup> century the North Atlantic SST has emerged as a  
507 dominant player in controlling dust activity over South Asia, in contrast to the hitherto important role played by  
508 the Pacific SST. This is accompanied by the resumption of global warming following the early 21<sup>st</sup> century



509 warming hiatus and by persistent positive phases of NAO which has resulted in positive (cold) phase of the  
510 North Atlantic SST tripole pattern. Specifically, high dust activity during 2011-2018 is associated with negative  
511 SST anomaly over sub-tropical North Atlantic and positive SST anomaly over mid-latitude North Atlantic, the  
512 two southern arms of the North Atlantic SST tripole. The difference in SST between these two arms of the  
513 tripole, which we term as North Atlantic Difference Index or NADI, projects in to the SEA-like circulation  
514 anomaly during May to September months of 2001-2010. Interestingly, during 2011-2018 a weakening of the  
515 relation between NAO and NADI dilutes the impact of NADI on SEA. The result is a weakening of the South  
516 Asian monsoon which leads to decreased precipitation and general increase in dryness with enhanced dust load.  
517 Additionally, positive sea level pressure anomaly over South and Southwest Asia leads to anomalous northerlies  
518 and westerlies which are responsible for transporting dust over South Asia. Sensitivity studies conducted with  
519 CESM model shows that averaged for May-September the North Atlantic SST tripole anomaly can lead to  
520 around 10% increase in dust optical depth, while it can contribute to 30% increase in dust optical depth during  
521 the month of June. Most of the increase in dust load can be attributed to enhanced transport at 800 hPa pressure  
522 level, which increases dust concentration by 20% for May-September and by as much as 40-50% during May-  
523 June.

524 The present study demonstrates impact of the North Atlantic Ocean using 18 years of satellite data. However, in  
525 the past, cold events in the North Atlantic have been associated with the slowdown of the South Asian monsoon  
526 system and increase in dust fluxes over the northern Indian Ocean and Southwest Asia (e.g., Pourmand et al.,  
527 2004; Mohtadi et al., 2014; Safaierad et al., 2020). Longer term data needs to be analysed from recent past to  
528 better understand how this relation between dust and North Atlantic SST has fluctuated over time. This will  
529 provide important clues as to how future relative changes in global SST in a warming world can control dust  
530 fluxes over South Asia and the possible climate implications.

531

#### 532 **Code availability**

533 The code for CESM1.2 is available at <https://www.cesm.ucar.edu/models/cesm1.2/>

#### 534 **Data availability**

535 Level 3 MODIS Aqua+Terra version 6.1 daily aerosol data was downloaded from Level 1 and Atmosphere  
536 Archive and Distribution System (LAADS) Distributed Active Archive Center (DAAC) website  
537 (<https://ladsweb.modaps.eosdis.nasa.gov/missions-and-measurements/science-domain/l3-atmosphere>). IASI dust  
538 optical depth was obtained from [https://iasi.aeris-data.fr/dust-aod\\_iasi\\_a\\_data/](https://iasi.aeris-data.fr/dust-aod_iasi_a_data/). NCEP/NCAR meteorological  
539 fields, NOAA ERSST version 5 data, OISST version 2, COBE SST version 2 data and GPCP version 2.3  
540 precipitation data were obtained from National Oceanic and Atmospheric Administration (NOAA) Physical  
541 Sciences Laboratory website (<https://psl.noaa.gov/data/gridded/data.ncep.reanalysis.html>). Monthly PERSIANN  
542 precipitation data is maintained at University of California, Irvine (UCI), Center for Hydrometeorology and  
543 Remote Sensing (CHRS) website (<https://chrsdata.eng.uci.edu/>). Hurrell's station-based NAO data is available  
544 at <https://climatedataguide.ucar.edu/climate-data/hurrell-north-atlantic-oscillation-nao-index-station-based>.  
545 AERONET coarse mode aerosol data were obtained from <https://aeronet.gsfc.nasa.gov/>.



546 **Author contribution**

547 PB conceived the study, carried out model simulations, analyzed the data and wrote the manuscript. SKS and  
548 KKM contributed to scientific analysis and revision of the manuscript.

549 **Competing interests**

550 The authors declare that they have no conflict of interest.

551 **Special issue statement**

552 This article is part of the special issue “Interactions between aerosols and the South West Asian monsoon”. It is  
553 not associated with a conference.

554 **Acknowledgements**

555 This research is supported by the Ministry of Earth Sciences (grant no. MM/NERC-MoES-1/2014/002). PB is  
556 also supported by Department of Science and Technology INSPIRE Faculty scheme. We acknowledge the  
557 computational facilities provided by Supercomputer Education and Research Centre (SERC) at the Indian  
558 Institute of Science for carrying out CESM simulations.

559

560 **References**

561 Abish, B. and Mohanakumar, K.: Absorbing aerosol variability over the Indian subcontinent and its increasing  
562 dependence on ENSO, *Global Planet. Change*, 106, 13–19, <https://doi.org/10.1016/j.gloplacha.2013.02.007>,  
563 2013.

564 Albani, S., Mahowald, N. M., Perry, A. T., Scanza, R. A., Heavens, N. G., Zender, C. S., Maggi, V., Kok, J. F.,  
565 and Otto-Bliessner, B. L.: Improved dust representation in the Community Atmosphere Model. *J. Adv. Model.*  
566 *Earth Syst.*, 6, 541–570, <https://doi.org/10.1002/2013MS000279>, 2014.

567 Annamalai, H., Taguchi, B., McCreary, J. P., Nagura, M., and Miyama, T.: Systematic errors in South Asian  
568 monsoon simulation: Importance of equatorial Indian Ocean processes, *J. Climate*, 30, 8159–8178,  
569 <https://doi.org/10.1175/JCLI-D-16-0573.1>, 2017.

570 Ashok, K., Guan, Z., Saji, N. H., and Yamagata, T.: Individual and combined influences of ENSO and the  
571 Indian Ocean Dipole on the Indian Summer Monsoon, *J. Climate*, 17, 3141–3155, [https://doi.org/10.1175/1520-0442\(2004\)017<3141:IACIOE>2.0.CO;2](https://doi.org/10.1175/1520-0442(2004)017<3141:IACIOE>2.0.CO;2), 2004.

573 Ashouri, H., Hsu, K., Sorooshian, S., Braithwaite, D. K., Knapp, K. R., Cecil, L. D., Nelson, B. R., and Pratt,  
574 O. P.: PERSIANN-CDR: daily precipitation climate data record from multisatellite observations for  
575 hydrological and climate studies, *B. Am. Meteorol. Soc.*, 96, 69–83, <https://doi.org/10.1175/BAMS-D-13-00068.1>, 2015.



- 577 Barlow, M., Heidi, C., and Bradfield, L.: Drought in Central and Southwest Asia: La Niña, the Warm Pool, and  
578 Indian Ocean Precipitation, *J. Climate*, 15, 697–700, 2002.
- 579 Banerjee, P., and Kumar, S. P.: ENSO Modulation of Interannual Variability of Dust Aerosols over the  
580 Northwest Indian Ocean, *J. Climate*, 29, 1287–1303, <https://doi.org/10.1175/JCLI-D-15-0039.1>, 2016.
- 581 Banerjee, P., Satheesh, S. K., Krishnamoorthy, K., Nanjundiah, R. S., and Nair, V. S.: Long-Range Transport of  
582 Mineral Dust to the Northeast Indian Ocean: Regional versus Remote Sources and the Implications, *J. Climate*,  
583 32, 1525–1549, <https://doi.org/10.1175/JCLI-D-18-0403.1>, 2019.
- 584 Bjerknes, J.: Atlantic air-sea interaction, *Adv. Geophys.* 10, 1–82 [https://doi.org/10.1016/S0065-2687\(08\)](https://doi.org/10.1016/S0065-2687(08)60005-9)  
585 60005-9, 1964.
- 586 Bollasina, M. A., Ming, Y., and Ramaswamy, V.: Anthropogenic aerosols and the weakening of the South  
587 Asian summer monsoon, *Science*, 334, 502–505, <https://doi.org/10.1126/science.1204994>, 2011.
- 588 Boos, W. R. and Hurley, J. V.: Thermodynamic Bias in the Multimodel Mean Boreal Summer Monsoon, *J.*  
589 *Climate*, 26, 2279–2287, <https://doi.org/10.1175/jcli-d-12-00493.1>, 2013.
- 590 Capelle, V., Chédin, A., Pondrom, M., Crevoisier, C., Armante, R., Crepeau, L., and Scott, N.: Infrared dust  
591 aerosol optical depth retrieved daily from IASI and comparison with AERONET over the period 2007–2016,  
592 *Remote Sens. Environ.*, 206, 15–32, <https://doi.org/10.1016/j.rse.2017.12.008>, 2018.
- 593 Chang, C., Harr, P., and Ju, J.: Possible Roles of Atlantic Circulations on the Weakening Indian Monsoon  
594 Rainfall–ENSO Relationship, *J. Climate*, 14, 2376–2380, [https://doi.org/10.1175/1520-](https://doi.org/10.1175/1520-0442(2001)014<2376:PROACO>2.0.CO;2)  
595 0442(2001)014<2376:PROACO>2.0.CO;2, 2001.
- 596 Chattopadhyay, R., Phani, R., Sabeerali, C. T., Dhakate, A. R., Salunke, K. D., Mahapatra, S., Suryachandra  
597 Rao, A., and Goswami, B. N.: Influence of extratropical sea-surface temperature on the Indian summer  
598 monsoon: An unexplored source of seasonal predictability, *Quart. J. Roy. Meteor. Soc.*, 141, 2760–2775,  
599 <https://doi.org/10.1002/qj.2562>, 2015.
- 600 Delworth, T. L., Zeng, F., Vecchi, G. A., Yang, X., Zhang, L., and Zhang, R.: The North Atlantic Oscillation as  
601 a driver of rapid climate change in the Northern Hemisphere, *Nat. Geosci.*, 9, 509–513,  
602 <https://doi.org/10.1038/ngeo2738>, 2016.
- 603 Deser, C., Guo, R., and Lehner, F.: The relative contributions of tropical Pacific sea surface temperatures and  
604 atmospheric internal variability to the recent global warming hiatus, *Geophys. Res. Lett.*, 44, 7945–7954,  
605 <https://doi.org/10.1002/2017GL074273>, 2017a.
- 606 Deser, C., Hurrell, J. W., and Phillips, A.S.: The role of the North Atlantic Oscillation in European climate  
607 projections, *Clim. Dynam.*, 49, 3141–3157, <https://doi.org/10.1007/s00382-016-3502-z>, 2017b.



- 608 Deepshikha, S., Satheesh, S. K., and Srinivasan, J.: Dust aerosols over India and adjacent continents retrieved  
609 using METEOSAT infrared radiance Part II: quantification of wind dependence and estimation of radiative  
610 forcing, *Annales Geophysicae*, 24, 63–79, doi:10.5194/angeo-24-63-2006, 2006.
- 611 England, M. H., McGregor, S., Spence, P., Meehl, G. A., Timmermann, A., Cai, W., Gupta, A. S., McPhaden,  
612 M. J., Purich, A., and Santoso, A.: Recent intensification of wind-driven circulation in the Pacific and the on-  
613 going warming hiatus, *Nat. Clim. Change*, 4, 222–227, <https://doi.org/10.1038/nclimate2106>, 2014.
- 614 Feng, S. and Hu, Q.: How the North Atlantic Multidecadal Oscillation may have influenced the Indian summer  
615 monsoon during the past two millennia?, *Geophys. Res. Lett.*, 35, L01707, doi:10.1029/2007GL032484, 2008.
- 616 Folland, C. K., Knight, J., Linderholm, H. W., Fereday, D., Ineson, S., and Hurrell, J. W.: The summer North  
617 Atlantic Oscillation: past, present, and future, *J. Climate*, 22, 1082–1103, 2009.
- 618 Gao, M., Sherman, P., Song, S., Yu, Y., Wu, Z., and McElroy, M. B.: Seasonal prediction of Indian wintertime  
619 aerosol pollution using the ocean memory effect, *Sci. Adv.*, 5, eaav4157,  
620 <https://doi.org/10.1126/sciadv.aav4157>, 2019.
- 621 Gao, Y., Wang, H. J., and Chen, D.: Interdecadal variations of the South Asian summer monsoon circulation  
622 variability and the associated sea surface temperatures on interannual scales, *Adv. Atmos. Sci.*, 34, 816–832,  
623 <https://doi.org/10.1007/s00376-017-6246-8>, 2017.
- 624 Gastineau, G. and Frankignoul, C.: Influence of the North Atlantic SST Variability on the Atmospheric  
625 Circulation during the Twentieth Century, *J. Climate*, 28, 1396–1416, <https://doi.org/10.1175/JCLI-D-14-00424.1>, 2015.
- 627 Ginoux, P., Prospero, J. M., Gill, T. E., Hsu, N. C., and Zhao, M.: Global-scale attribution of anthropogenic and  
628 natural dust sources and their emission rates based on MODIS Deep Blue aerosol products, *Rev. Geophys.*, 50,  
629 RG3005, doi:10.1029/2012RG000388, 2012.
- 630 Goswami, B. N., Madhusoodanan, M., Neema, C., and Sengupta, D.: A physical mechanism for North Atlantic  
631 SST influence on the Indian summer monsoon, *Geophys. Res. Lett.*, 33, L02706,  
632 <https://doi.org/10.1029/2005GL024803>, 2006.
- 633 Han, Z., Luo, F.F., and Wan, J.H.: The observational influence of the North Atlantic SST tripole on the early  
634 spring atmospheric circulation, *Geophys. Res. Lett.*, 43, 2998–3003, <https://doi.org/10.1002/2016GL068099>,  
635 2016.
- 636 Hanf, F. S., and Annamalai, H.: Systematic Errors in South Asian Monsoon Precipitation: Process-Based  
637 Diagnostics and Sensitivity to Entrainment in NCAR Models, *J. Climate*, 33, 2817–2840,  
638 <https://doi.org/10.1175/JCLI-D-18-0495.1>, 2020.
- 639 Hirahara, S., Ishii, M., and Fukuda, Y.: Centennial-scale sea surface temperature analysis and its uncertainty, *J.*  
640 *Climate*, 27, 57–75, <https://doi.org/10.1175/JCLI-D-12-00837.1>, 2014.



- 641 Hsu, N. C., Tsay, S. C., King, M. D., and Herman, J. R.: Aerosol Properties over Bright-Reflecting Source  
642 Regions, *IEEE T. Geosci. Remote*, 42, 557–569, <https://doi.org/10.1109/TGRS.2004.824067>, 2004.
- 643 Hsu, N. C., Tsay, S.-C., King, M. D., and Herman, J. R.: Deep Blue retrievals of Asian aerosol properties during  
644 ACE-Asia, *IEEE T. Geosci. Remote Sens.*, 44, 3180–3195, <https://doi.org/10.1109/TGRS.2006.879540>, 2006.
- 645 Hu, S., and Fedorov, A.V.: The extreme El Niño of 2015–2016 and the end of global warming hiatus, *Geophys.*  
646 *Res. Lett.*, 44, 3816–3824, doi:10.1002/2017GL072908, 2017.
- 647 Huang B., Thorne, P. W., Banzon, V. F., Boyer, T., Chepurin, G., Lawrimore, J. H., Menne, M. J., Smith, T. M.,  
648 Vose, R. S., and Zhang, H-M.: Extended Reconstructed Sea Surface Temperature, Version 5 (ERSSTv5):  
649 Upgrades, Validations, and Intercomparisons, *J. Climate*, 30, 8179–8205, doi: 10.1175/JCLI-D-16-0836.1,  
650 2017.
- 651 Huang, X., Zhou, T., Turner, A., Dai, A., Chen, X., Clark, R., and Zou, L.: The Recent Decline and Recovery of  
652 Indian Summer Monsoon Rainfall: Relative Roles of External Forcing and Internal Variability, *J. Climate*, 33,  
653 5035-5060, doi:10.1175/jcli-d-19-0833.1, 2020.
- 654 Huffman, G. J., Alder, R. F., Arkin, P., Chang, A., Ferraro, R., Gruber, A., Janowiak, J., McNab, A., Rudolf, B.,  
655 and Schneider, U.: The Global Precipitation Climatology Project (GPCP) Combined Precipitation Dataset, *B.*  
656 *Am. Meteorol. Soc.*, 78, 5–20, [https://doi.org/10.1175/1520-0477\(1997\)078<0005:TGPCPG>2.0.CO;2](https://doi.org/10.1175/1520-0477(1997)078<0005:TGPCPG>2.0.CO;2), 1997.
- 657 Hurrell, J. W.: Decadal trends in the North Atlantic oscillation: Regional temperatures and precipitation,  
658 *Science*, 269, 676–679, <https://doi.org/10.1126/science.269.5224.676>, 1995.
- 659 Hurrell, J. W., Hack, J. J., Shea, D., Caron, J. M., and Rosinski, J.: A New Sea Surface Temperature and Sea Ice  
660 Boundary Dataset for the Community Atmosphere Model, *J. Climate*, 21, 5145–5153,  
661 <https://doi.org/10.1175/2008JCLI2292.1>, 2008.
- 662 Hurrell, J. W., and Deser C.: North Atlantic climate variability: the role of the North Atlantic Oscillation, *J.*  
663 *Marine Syst.*, 79(3), 231-244, <https://doi.org/10.1016/j.jmarsys.2009.11.002>, 2009.
- 664 Iles, C., and Hegerl, G.: Role of the North Atlantic Oscillation in decadal temperature trends, *Environ. Res.*  
665 *Lett.*, 12, 114010, <https://doi.org/10.1088/1748-9326/aa9152>, 2017.
- 666 Jin, Q., Wei, J., and Yang, Z.-L.: Positive response of Indian summer rainfall to Middle East dust, *Geophys.*  
667 *Res. Lett.*, 41, 4068–4074, <https://doi.org/10.1002/2014GL059980>, 2014.
- 668 Jin, Q., Wei, J., Pu, B., Yang, Z. L., and Parajuli, S. P.: High summertime aerosol loadings over the Arabian Sea  
669 and their transport pathways, *J. Geophys. Res.- Atmos.*, 123, 10568–10590,  
670 <https://doi.org/10.1029/2018jd028588>, 2018a.
- 671 Jin, Q., and Wang, C.: The greening of Northwest Indian subcontinent and reduction of dust abundance resulting  
672 from Indian summer monsoon revival, *Sci Rep.*, 8, 4573, <https://doi.org/10.1038/s41598-018-23055-5>, 2018b.



- 673 Kalnay, E., Kanamitsu, M., Kistler, R., Collins, W., Deaven, D., Gandin, L., Iredell, M., Saha, S., White, G.,  
674 Woollen, J., Zhu, Y., Leetmaa, A., Reynolds, R., Chelliah, M., Ebisuzaki, W., Higgins, W., Janowiak, J., Mo, K.  
675 C., Ropelewski, C., and Wang, J.: The NCEP/NCAR 40-year reanalysis project, *B. Am. Meteorol. Soc.*, 77,  
676 437–471, doi:10.1175/1520-0477(1996)077<0437:Tnyrp>2.0.Co;2, 1996.
- 677 Kim, M.-K., Lau, W. K. M., Kim, K.-M., Sang, J., Kim, Y.-H., and Lee, W.-S.: Amplification of ENSO effects  
678 on Indian summer monsoon by absorbing aerosols, *Clim. Dynam.*, 46, 2657–2671,  
679 <https://doi.org/10.1007/s00382-015-2722-y>, 2016.
- 680 Kinter III, J., Miyakoda, K., and Yang, S.: Recent change in the connection from the Asian monsoon to ENSO,  
681 *J. Climate*, 15, 1203–1215, [https://doi.org/10.1175/1520-0442\(2002\)015<1203:RCITCF>2.0.CO;2](https://doi.org/10.1175/1520-0442(2002)015<1203:RCITCF>2.0.CO;2), 2002.
- 682 Kosaka, Y., and Xie, S. P.: Recent global-warming hiatus tied to equatorial Pacific surface cooling, *Nature*, 501,  
683 403–407, doi:<https://doi.org/10.1038/nature12534>, 2013.
- 684 Kosaka, Y., and Xie, S. P.: The tropical Pacific as a key pacemaker of the variable rates of global warming,  
685 *Nat. Geosci.*, 9, 669–673, doi:10.1038/ngeo2770, 2016.
- 686 Krishnamurthy, L., and Krishnamurthy, V.: Teleconnections of Indian monsoon rainfall with AMO and Atlantic  
687 tripole, *Clim. Dynam.*, 46, 2269–2285, doi:<https://doi.org/10.1007/s00382-015-2701-3>, 2015.
- 688 Kucharski, F., Bracco, A., Yoo, J. H., and Molteni, F.: Low-frequency variability of the Indian monsoon –  
689 ENSO relation and the Tropical Atlantic: the “weakening” of the ’80s and ’90s, *J. Climate*, 20, 4255–4266,  
690 <https://doi.org/10.1175/JCLI4254.1>, 2007.
- 691 Kucharski, F., Bracco, A., Yoo, J. H., and Molteni, F.: Atlantic forced component of the Indian monsoon  
692 interannual variability, *Geophys. Res. Lett.*, 35, L04706, doi:10.1029/2007GL033037, 2008.
- 693 Kumar, K. K., Rajagopalan, B., and Cane, K. A.: On the weakening relationship between the Indian Monsoon  
694 and ENSO, *Science*, 284, 2156–2159, <https://doi.org/10.1126/science.284.5423.2156>, 1999.
- 695 Kumar, K. K., Rajagopalan, B., Hoerling, M., Bates, G., Cane, M. A.: Unraveling the Mystery of Indian  
696 Monsoon Failure During El Niño, *Science*, 314, 115–119, <https://doi.org/10.1126/science.1131152>, 2006.
- 697 Lee, T. and McPhaden, M. J.: Increasing intensity of El Niño in the central –equatorial Pacific, *Geophys. Res.*  
698 *Lett.*, 37, L14603, <https://doi.org/10.1029/2010GL044007>, 2010.
- 699 Liu, W., Fedorov, A. V., Xie, S. P., and Hu, S.: Climate impacts of a weakened Atlantic Meridional Overturning  
700 Circulation in a warming climate, *Sci. Adv.*, 6, eaaz4876, <https://doi.org/10.1126/sciadv.aaz4876>, 2020.
- 701 Mahowald, N. M., Muhs, D. R., Levis, S., Rasch, P. J., Yoshioka, M., Zender, C. S., and Luo, C.: Change in  
702 atmospheric mineral aerosols in response to climate: Last glacial period, preindustrial, modern, and doubled  
703 carbon dioxide climates, *J. Geophys. Res.*, 111, D10202, <https://doi.org/10.1029/2005JD006653>, 2006.



- 704 Mariotti, A., Zeng, N., and Lau, K.-M.: Euro-Mediterranean rainfall and ENSO – a seasonally varying  
705 relationship, *Geophys. Res. Lett.*, 29, 1621–1625, doi:10.1029/2001GL014248, 2002.
- 706 Marticorena, B., and Bergametti, G.: Modeling the atmospheric dust cycle. 1. Design of a soil-derived emission  
707 scheme, *J. Geophys. Res. - Atmos.*, 100, 16415–16430, 1995.
- 708 Mohtadi, M., Prange, M., Oppo, D. W., De Pol-Holz, R., Merkel, U., Zhang, X., Steinke, S., and Lückge, A.:  
709 North Atlantic forcing of tropical Indian Ocean climate, *Nature*, 509, 76–80, 2014.
- 710 Neale, R. B., Richter, J. H., Conley, A. J., Park, S., Lauritzen, P. H., and Gettleman, A.: Description of the  
711 NCAR Community Atmosphere Model (CAM 4.0), NCAR Tech. Note NCAR/TN-485+STR, 212 pp.,  
712 www.cesm.ucar.edu/models/ccsm4.0/cam/docs/description/cam4\_desc.pdf, 2010.
- 713 Notaro, M., Yu, Y., and Kalashnikova, O. V.: Regime shift in Arabian dust activity, triggered by persistent  
714 fertile crescent drought, *J. Geophys. Res. - Atmos.*, 120, 10229–10249, <https://doi.org/10.1002/2015JD023855>,  
715 2015.
- 716 Osborne, J. M., Collins, M., Screen, J. A., Thomson, S. I., and Dunstone, N.: The North Atlantic as a Driver of  
717 Summer Atmospheric Circulation, *J. Climate*, 33, 7335–7351, <https://doi.org/10.1175/JCLI-D-19-0423.1>, 2020.
- 718 Ossó, A., Sutton, R., Shaffrey, L., and Dong, B.: Observational evidence of European summer weather patterns  
719 predictable from spring, *Proc. Natl. Acad. Sci. USA*, 115, 59–63, <https://doi.org/10.1073/pnas.1713146114>,  
720 2018.
- 721 Ossó, A., Sutton, R., Shaffrey, L., and Dong, B.: Development, Amplification, and Decay of Atlantic/European  
722 Summer Weather Patterns Linked to Spring North Atlantic Sea Surface Temperatures, *J. Climate*, 33, 5939–  
723 5951, <https://doi.org/10.1175/JCLI-D-19-0613.1>, 2020.
- 724 Pandey, S. K., Vinoj, V., Landu, K., and Babu, S. S.: Declining pre-monsoon dust loading over South Asia:  
725 Signature of a changing regional climate, *Sci. Rep.*, 7, 16062, <https://doi.org/10.1038/s41598-017-16338-w>,  
726 2017.
- 727 Pandithurai, G., Dipu, S., Dani, K. K., Tiwari, S., Bisht, D. S., Devara, P. C. S., and Pinker, R. T.: Aerosol  
728 radiative forcing during dust events over New Delhi, India, *J. Geophys. Res.*, 113, D13209,  
729 doi:10.1029/2008JD009804, 2008.
- 730 Pourmand, A., Marcantonio, F., and Schulz, H.: Variations in productivity and eolian fluxes in the northeastern  
731 Arabian Sea during the past 110 ka, *Earth Planet. Sci. Lett.*, 221, 39–54, doi:10.1016/S0012-821X(04)00109-8,  
732 2004.
- 733 Pu, B. and Ginoux, P.: The impact of the Pacific Decadal Oscillation on springtime dust activity in Syria,  
734 *Atmos. Chem. Phys.*, 16, 13431–13448, <https://doi.org/10.5194/acp-16-13431-2016>, 2016.
- 735 Pu, B. and Ginoux, P.: How reliable are CMIP5 models in simulating dust optical depth?, *Atmos. Chem. Phys.*,  
736 18, 12491–12510, <https://doi.org/10.5194/acp-18-12491-2018>, 2018.



- 737 Rajeevan, M., and Pai, D.S.: On the El Niño-Indian monsoon predictive relationships, *Geophys. Res. Lett.*, 34,  
738 L04704, doi:10.1029/2006GL028916, 2007.
- 739 Rajeevan, M., and Sridhar, L.: Inter-annual relationship between Atlantic sea surface temperature anomalies and  
740 Indian summer monsoon, *Geophys. Res. Lett.*, 35, L21704, doi:10.1029/2008GL036025, 2008.
- 741 Ramanathan, V., Chung, C., Kim, D., Bettge, T., Buja, L., Kiehl, J. T., Washington, W. M., Fu, Q., Sikka, D. R.,  
742 and Wild, M.: Atmospheric brown clouds: Impacts on South Asian climate and hydrological cycle, *P. Natl.*  
743 *Acad. Sci. USA*, 102, 5326–5333, <https://doi.org/10.1073/pnas.0500656102>, 2005.
- 744 Rasmusson, E. M., and Carpenter, T.H.: The relationship between eastern equatorial Pacific sea surface  
745 temperatures and rainfall over India and Sri Lanka, *Mon. Weather Rev.*, 111, 517–528, 1983.  
746
- 747 Reynolds, R. W., Rayner, N. A., Smith, T. M., Stokes, D. C., and Wang, W.: An improved in situ and satellite  
748 SST analysis for climate, *J. Climate*, 15, 1609–1625, [https://doi.org/10.1175/1520-0442\(2002\)015<1609:AIISAS>2.0.CO;2](https://doi.org/10.1175/1520-0442(2002)015<1609:AIISAS>2.0.CO;2), 2002.  
749
- 750 Rodwell, M. J., Rowell, D. P., and Folland, C. K.: Oceanic forcing of the wintertime North Atlantic Oscillation  
751 and European climate, *Nature*, 398, 320–323, <https://doi.org/10.1038/18648>, 1999.
- 752 Sabeerali, C. T., Ajayamohan, R. S., Bangalath, H. K., and Chen, N.: Atlantic Zonal Mode: an emerging source  
753 of Indian summer monsoon variability in a warming world, *Geophys. Res. Lett.*, 46, 4460–4464,  
754 <https://doi.org/10.1029/2019GL082379>, 2019.
- 755 Safaierad, R., Mohtadi, M., Zolitschka, B., Yokoyama, Y., Vogt, C., Schefuß, E.: Elevated dust depositions in  
756 West Asia linked to ocean–atmosphere shifts during North Atlantic cold events, *Proc. Natl. Acad. Sci. USA*, 117  
757 (31) 18272–18277, doi: 10.1073/pnas.2004071117, 2020.
- 758 Sanap, S. D., Ayantika, D. C., Pandithurai, G., and Niranjana, K.: Assessment of the aerosol distribution over  
759 Indian subcontinent in CMIP5 models, *Atmos. Environ.*, 87, 123–137,  
760 <https://doi.org/10.1016/j.atmosenv.2014.01.017>, 2014.
- 761 Satheesh, S. K., and Ramanathan, V.: Large differences in tropical aerosol forcing at the top of the atmosphere  
762 and Earth's surface, *Nature*, 405, 60–63, 2000.
- 763 Sikka, D. R.: Some aspects of the large scale fluctuations of summer monsoon rainfall over India in relation to  
764 fluctuations in the planetary and regional scale circulation parameters, *Proc. Ind. Acad. Sci. (Earth & Planet.*  
765 *Sci.)*, 89, 179–195, 1980.
- 766 Solmon, F., Nair, V. S., and Mallet, M.: Increasing Arabian dust activity and the Indian summer monsoon,  
767 *Atmos. Chem. Phys.*, 15, 8051–8064, doi:10.5194/acp-15-8051-2015, 2015.
- 768 Sperber, K. R., Annamalai, H., Kang, I.-S., Kitoh, A., Moise, A., Turner, A., Wang, B., and Zhou, T.: The Asian  
769 summer monsoon: an intercomparison of CMIP5 vs. CMIP3 simulations of the late 20th century, *Clim. Dynam.*,  
770 41, 2711–2744, <https://doi.org/10.1007/s00382-012-1607-6>, 2013.



- 771 Srivastava, A. K., Rajeevan, M., and Kulkarni, R.: Teleconnection of OLR and SST anomalies over Atlantic  
772 Ocean with Indian summer monsoon, *Geophys. Res. Lett.*, 29(8), 1284, doi:10.1029/2001GL013837, 2002.
- 773 Srivastava, G., Chakraborty, A., and Nanjundiah, R.S.: Multidecadal see-saw of the impact of ENSO on Indian  
774 and West African summer monsoon rainfall, *Clim Dynam.*, 52, 6633–6649, doi:10.1007/s00382-018-4535-2,  
775 2019.
- 776 Stocker, T. F., Qin, D., Plattner, G.-K., Tignor, M., Allen, S. K., Boschung, J., Nauels, A., Xia, Y., Bex, V., and  
777 Midgley, P. M.: *Climate Change 2013: The Physical Science Basis. Contribution of Working Group I to the  
778 Fifth Assessment Report of the Inter-governmental Panel on Climate Change*, Cambridge University Press,  
779 2013.
- 780 Trenberth, K. E. and Fasullo, J. T.: An apparent hiatus in global warming?, *Earth's Future*, 1, 19–32,  
781 <https://doi.org/10.1002/2013EF000165>, 2013.
- 782 Trenberth, K. E., Fasullo, J. T., Branstator, G., and Phillips, A. S.: Seasonal aspects of the recent pause in  
783 surface warming, *Nat. Clim. Change*, 4, 911–916, doi:10.1038/nclimate2341, 2014.
- 784 Thompson, L. G., Yao, T., Mosley-Thompson, E., Davis, M. E., Henderson, K. A., and Lin, P. N.: A high-  
785 resolution millennial record of the South Asian Monsoon from Himalayan ice cores, *Science*, 289, 1916–1919,  
786 2000.
- 787 Vinoj, V., Rasch, P., Wang, H., Yoon, J., Ma, P., Landu, K., and Singh, B.: Short-term modulation of Indian  
788 summer monsoon rainfall by West Asian dust, *Nat. Geosci.*, 7, 308–313, <https://doi.org/10.1038/ngeo2107>,  
789 2014.
- 790 Visbeck, M., Cullen, H., Krahnmann, G., and Naik, N.: An ocean model's response to North Atlantic Oscillation-  
791 like wind forcing, *Geophys. Res. Lett.*, 25, 4521–4524, 1998.
- 792 Visbeck, M. H., Hurrell, J. W., Polvani, L., and Cullen, H. M.: The North Atlantic Oscillation: past, present and  
793 future, *P. Natl. Acad. Sci. USA*, 98, 12876–12877, 2001.
- 794 Walker, A. L., Liu, M., Miller, S. D., Richardson, K. A., and Westphal, D. L.: Development of a dust source  
795 database for mesoscale forecasting in southwest Asia, *J. Geophys. Res.*, 114, D18207,  
796 doi:10.1029/2008JD011541, 2009.
- 797 Wulff, C. O., Greatbatch, R. J., Domeisen, D. I. V., Gollan, G., and Hansen, F.: Tropical forcing of the summer  
798 east Atlantic pattern, *Geophys. Res. Lett.*, 44, 11 166–11 173, <https://doi.org/10.1002/2017GL075493>, 2017.
- 799 Xie, S.-P., and Kosaka, Y.: What caused the global surface warming hiatus of 1998–2013? *Curr. Climate  
800 Change Rep.*, 3, 128–140, <https://doi.org/10.1007/s40641-017-0063-0>, 2017.
- 801 Yeh, S.-W., Kug, J.-S., Dewitte, B., Kwon, M.-H., Kirtman, B.P., and Jin, F.-F.: El Niño in a changing climate,  
802 *Nature*, 461, 511–514, 2009.



- 803 Yu, Y., Notaro, M., Liu, Z., Wang, F., Alkolibi, F., Fadda, E., and Bakhrjy, F.: Climatic controls on the  
804 interannual to decadal variability in Saudi Arabian dust activity: toward the development of a seasonal dust  
805 prediction model, *J. Geophys. Res.- Atmos.*, 120, 1739–1758, <https://doi.org/10.1002/2014JD022611>, 2015.
- 806 Zender, C. S., Bian, H., and Newman, D.: Mineral Dust Entrainment and Deposition (DEAD) model:  
807 Description and 1990s dust climatology, *J. Geophys. Res.-Atmos.*, 108, 4416,  
808 <https://doi.org/10.1029/2002JD002775>, 2003a.
- 809 Zender, C. S., Newman, D., and Torres, O.: Spatial heterogeneity in aeolian erodibility: uniform, topographic,  
810 geomorphic and hydrologic hypotheses, *J. Geophys. Res.*, 108, 4543, doi:10.1029/2002JD003039, 2003b.
- 811 Zhang, R. and Delworth, T. L.: Impact of Atlantic multidecadal oscillations on India/Sahel rainfall and Atlantic  
812 hurricanes, *Geophys. Res. Lett.*, 33, L17712, doi:10.1029/2006GL026267, 2006.
- 813 Zhu, A., Ramanathan, V., Li, F., and Kim, D.: Dust plumes over the Pacific, Indian, and Atlantic oceans:  
814 climatology and radiative impact, *J. Geophys. Res.*, 112, D16208, doi:10.1029/2007JD008427, 2007.
- 815